Author's reply to:

"Effects of upper mantle heterogeneities on lithospheric stress field and dynamic topography" by Anthony Osei Tutu et al.

Referee #1 - Anonymous

Received and published: 20 November 2017

This paper presents a new mantle flow model that couples global mantle flow (driven by density heterogeneity inferred from seismic tomography) to a detailed surface model for the upper 300 km of the mantle – this includes more detailed heterogeneity associated with upper mantle viscosity variations and density heterogeneity. The authors use this coupled model to predict both lithospheric stresses and dynamic topography, which are both the result of convective stresses from viscous flow in the mantle. The authors use 2 different predictive flow models (TM1 based on heat flow and seafloor ages and TM2 based upper mantle tomography model) and compare them to the global stress map for stresses and 2 different predictions of dynamic topography. They find that both predictive flow models (which differ only in the upper 300 km) predict similar stress fields but TM2 gives a better prediction of dynamic topography. The authors conclude that dynamic topography is more sensitive to upper mantle structure than lithospheric stresses, that their model does a reasonably good job of predicting the lithospheric stress field, and that dynamic topography is better-predicted using seismic tomography data instead of heat flow and seafloor ages.

I think that the content of the paper useful and innovative – the new models are innovative and are – to my knowledge – the first of their kind to look at the impact of detailed upper mantle heterogeneity on stresses and dynamic topography. The predictions they make are useful for understanding the problem, and should lead to greater understanding of the system a. Thus, I think that the paper is eventually publishable.

We are very thankful to Referee #1 for his/her time and good recommendations and suggestions. We have attempted to address all of them in the revised manuscript as shown here below.

Ref 1: The paper has a lot of information and is a bit hard to follow because the authors are comparing 2 predictive models (TM1 and TM2) with 2 output fields (stresses and dynamic topography), one of which has 2 different options (dynamic topography from Steinberger 2016 or Hoggard 2016). Thus, there are several combinations of comparisons, and it is a bit of an effort to follow what is being compared with what. On top of that, the writing is a bit wordy with some repetition. This makes reading and understanding the paper a bit laborious.

I think for this paper to be effective, it needs better organization and structure, and the writing needs to be simplified and shortened. I give some suggestions for this below. Given this, I recommend significant re-revision of the figures and text, although I do not think that significant new analysis is necessary. Thus, I would probably call for "moderate revision". Below is a an overall assessment of the changes that I think would be useful for improving the paper and also some specific points about the paper.

AU: This is a very important suggestion, on the readability and understanding of our manuscript. Hence, we follow the referee's suggestions and have also re-organized the manuscript where it's necessary for easier reading.

Major Points:

Ref 2:
Overall Structure: One problem is that the predictions and analysis of stresses and dynamic topography are intermingled in section 3. I recommend separating this into two sections, one that is devoted to stresses and the other to dynamic topography. Thus, I recommend removing the topography predictions from Figs. 5 and 6 (so these figures are devoted to stresses), and removing the stresses from Fig. 7 (so this figure is for dynamic topography). I also recommend revising the text around these figures to focus specifically on stresses and then on dynamic topography.

AU: We have re-organized the manuscript to separate the reconstruction of the lithosphere stress field and dynamic topography together with the discussions around these reconstructions. The corresponding figures are also re-organized. Where necessary for the benefit of comparison and discussions with regards to the focus of the study, we have included and explained figures in the authors' response.

Ref 3:
Introduction – I think the introduction is a bit too long and rambling, and should get to the main point more quickly – that this paper presents a new method for evaluating the role of upper mantle heterogeneity (both density heterogeneity and viscosity heterogeneity) for mantle stresses. There is much background – condensing it to just the relevant parts will help the authors emphasize their new contribution a bit more clearly.

AU: We agree with this referee's suggestion to shorten the introduction and emphasize on the new approach our study presents. We have revised the introduction to make it short and concise with the focus on what is new with our study.

"See the attached tracked manuscript below"

Ref 4:
Conclusions – I think that the paper does a nice job of concluding the major results. But there is no discussion section – it would be helpful to have a short discussion of the implications of this work for our understanding of dynamic topography and stresses, and other factors that might be important to include in the models in the future.
AU: Since most of the discussions on the stress field and dynamic topography are presented in the respective extended sections in the chapter "Results and Discussion", we thought to rather give an extensive conclusion on the results.

Figures-There are more figures than are necessary. In particular:

Ref 5:
Figure 1 and 3 are illustrative about the model, but the information in these figures is not used much – perhaps only the essential components of Fig. 3 could be incorporated into Fig.1? (for example, the geoid, plate velocity, and tractions are not really used here)

AU: We combined the most relevant Figures in Figures 1 and 2 and also in Figures 3 and 4 resulting in the current new Figures 1 and 2 respectively, as shown below:

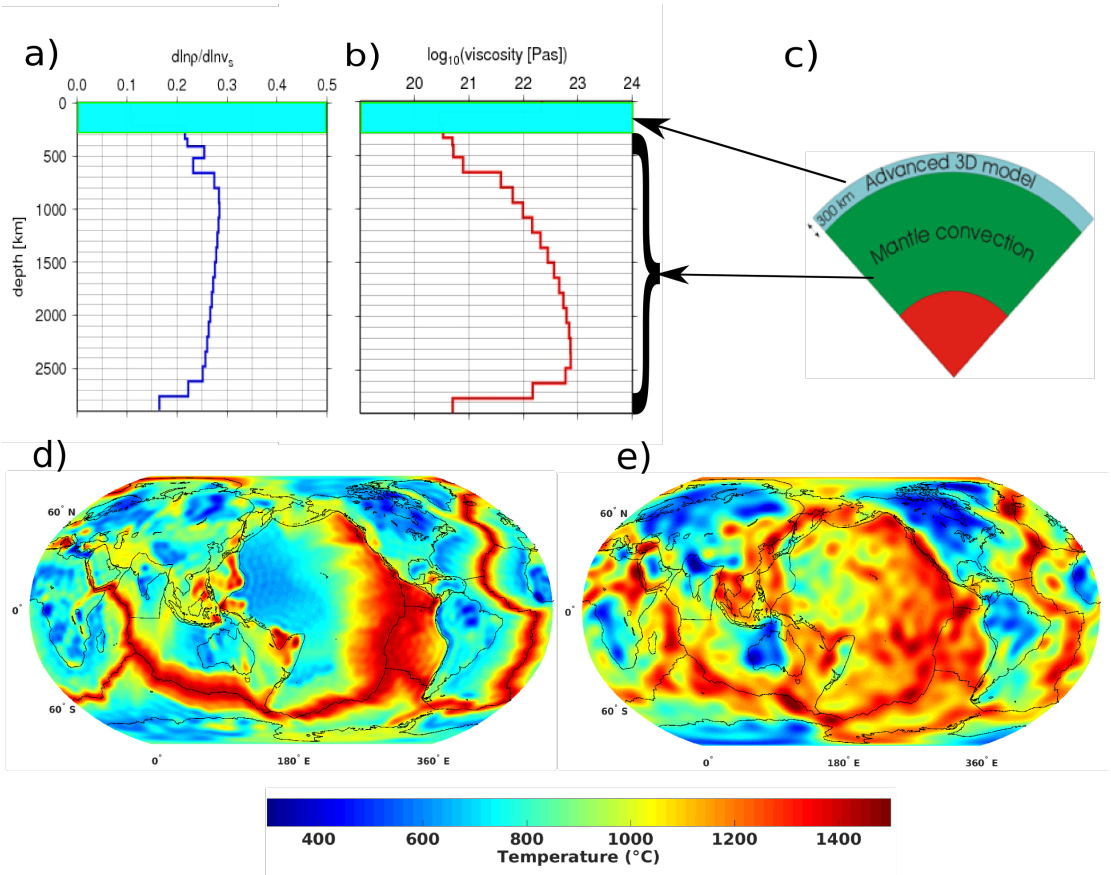

Figure 1: Adopted from Osei Tutu et al., (2017) (a) Depth-dependent scaling profile of S-wave velocity to density; (b) radial mantle viscosity structure (Steinberger and Calderwood, 2006) and (c) a schematic diagram of the numerical method that couples the 3D-lithosphere-asthenosphere code SLIM3D (Popov and Sobolev, 2008) to a lower mantle spectral flow code (Hager and O'Connell, 1981) at a depth of 300 km. The 3D thermal structure of the upper mantle (i.e. 300 km) at a depth of 80 km from two reference thermal models adopted in this study. d) TM1, a heat flow-based thermal structure inferred from the TC1 model of Artemieva (2006) in the continents and the sea floor age model of Müller et al. (2008) in the oceanic areas. e) TM2, the thermal structure of the upper mantle inferred from the S-wave tomography model SL2013sv of Schaeffer and Lebedev (2013). The "ring-ing" visible in the upper structure is a side effect introduced by smoothing sharp boundaries with a spherical harmonic expansion.

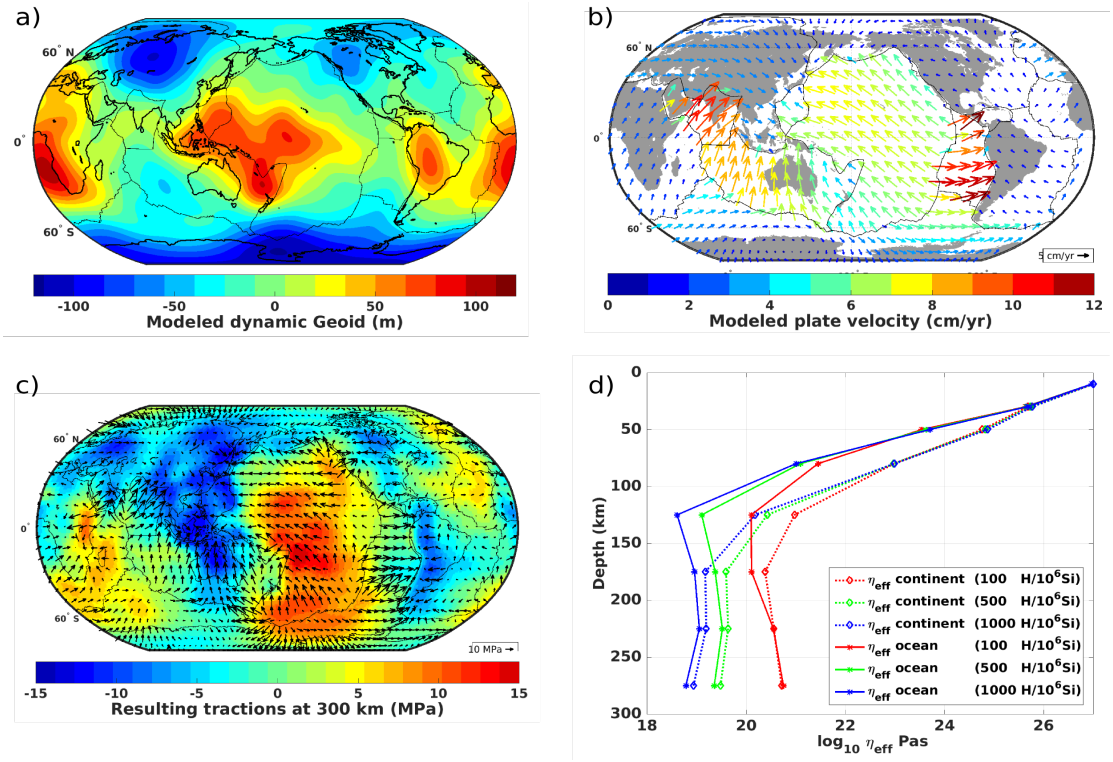

Figure 2: Modeled geoid anomaly and (b) modeled plate velocity, considering lateral viscosity variations with the TM1 thermal-density model in the upper 300 and a 3-D density structure of the mantle inferred from Becker and Boschi (2001) in combination with the layered viscosity profile from Steinberger and Calderwood (2006) imposed below 300 km. (c) Resulting total shear tractions at the 300 km depth generating stresses in the crust and lithospheric depth. (d) The corresponding average creep viscosity versus depth in the upper mantle (300 km) across continents and oceans, considering different olivine parameters.

NB:
Even though, Figure 2 is just illustrative of our model fitting other geophysical observables such as the geoid and plate motions (Figure 2a-b). Here also we maintain the figure with tractions to refer from the main text to what causes/generates the stresses in the lithosphere due to the viscous mantle flow.

Ref 6:

Figure 4 shows comparisons for different models of dislocation and diffusion creep, and different water contents – however it is not clear to me that all of this complexity is necessary? Why not simplify by showing only the most relevant models and say in the text what is the impact of changing the rheological parameters?

AU: We have combined the average resulting depth dependent creep viscosity into the geoid, plate motions and tractions figure. Shown above in Figure 2.

Ref 7:
As I mentioned above, I think that figures 5cd, 6cd, and 7cd are not necessary. Fig. 7 should be moved later into the dynamic topography section.

AU: We agree with the suggestion related to the previous version of Figures 5cd and 6cd, which have been moved to the supplementary information and are referred to

from the manuscript. However, we consider that Figures 7c-d (now Figures 8c-d) are important for carrying out our analysis of the influence of the crust on the stress field as compared to Figures 3&4(a-b) when we discuss the modeled topography.

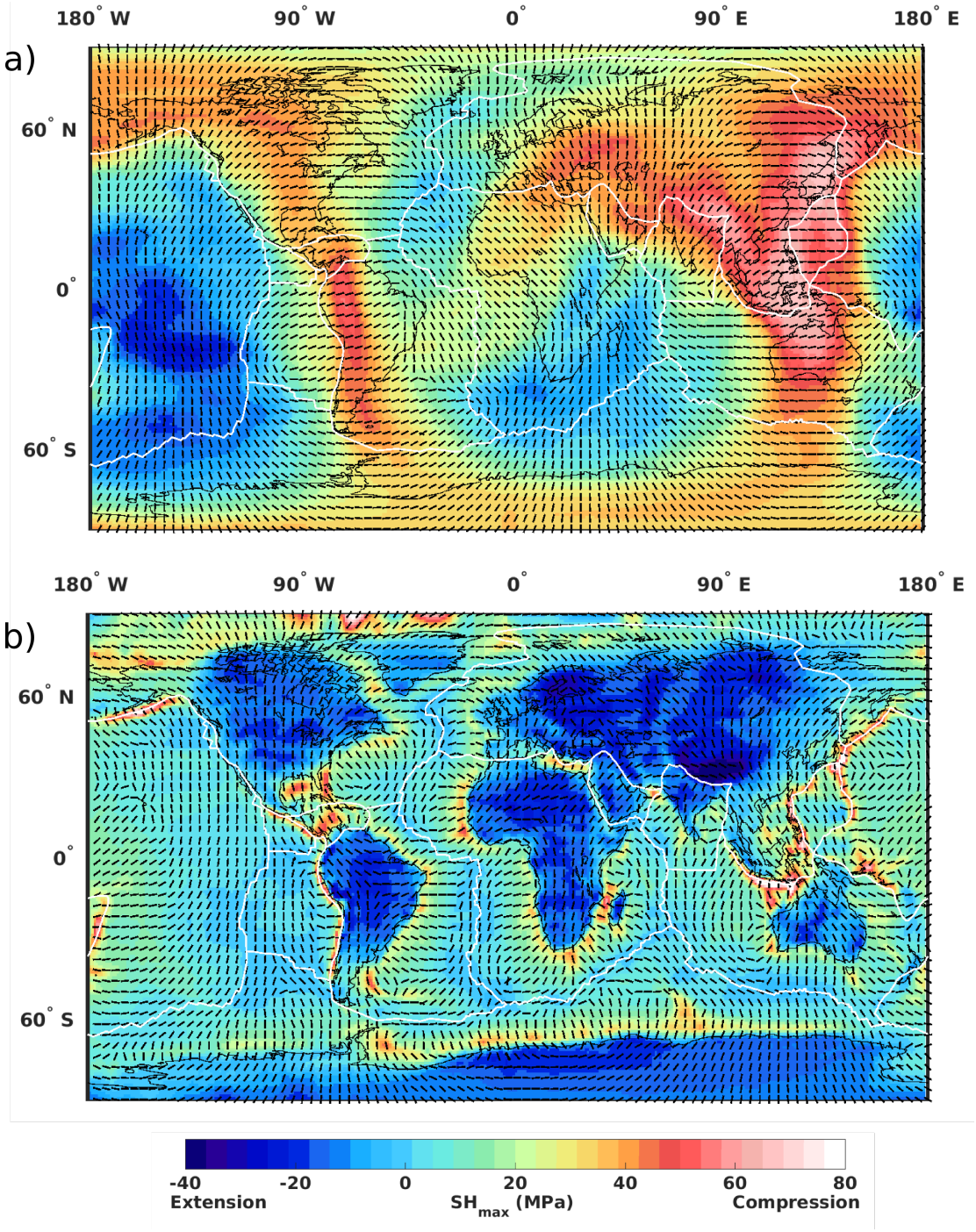

Figure3: a) Model-based maximum horizontal stress magnitude and most compressive stress directions [SHmax] following the convention with compression being positive, originating from mantle flow driven by density anomalies below 300 km. (b) Same for structure of the top 300 km of the upper mantle, computed with the CRUST 1.0 model and TM1 beneath air (free surface)

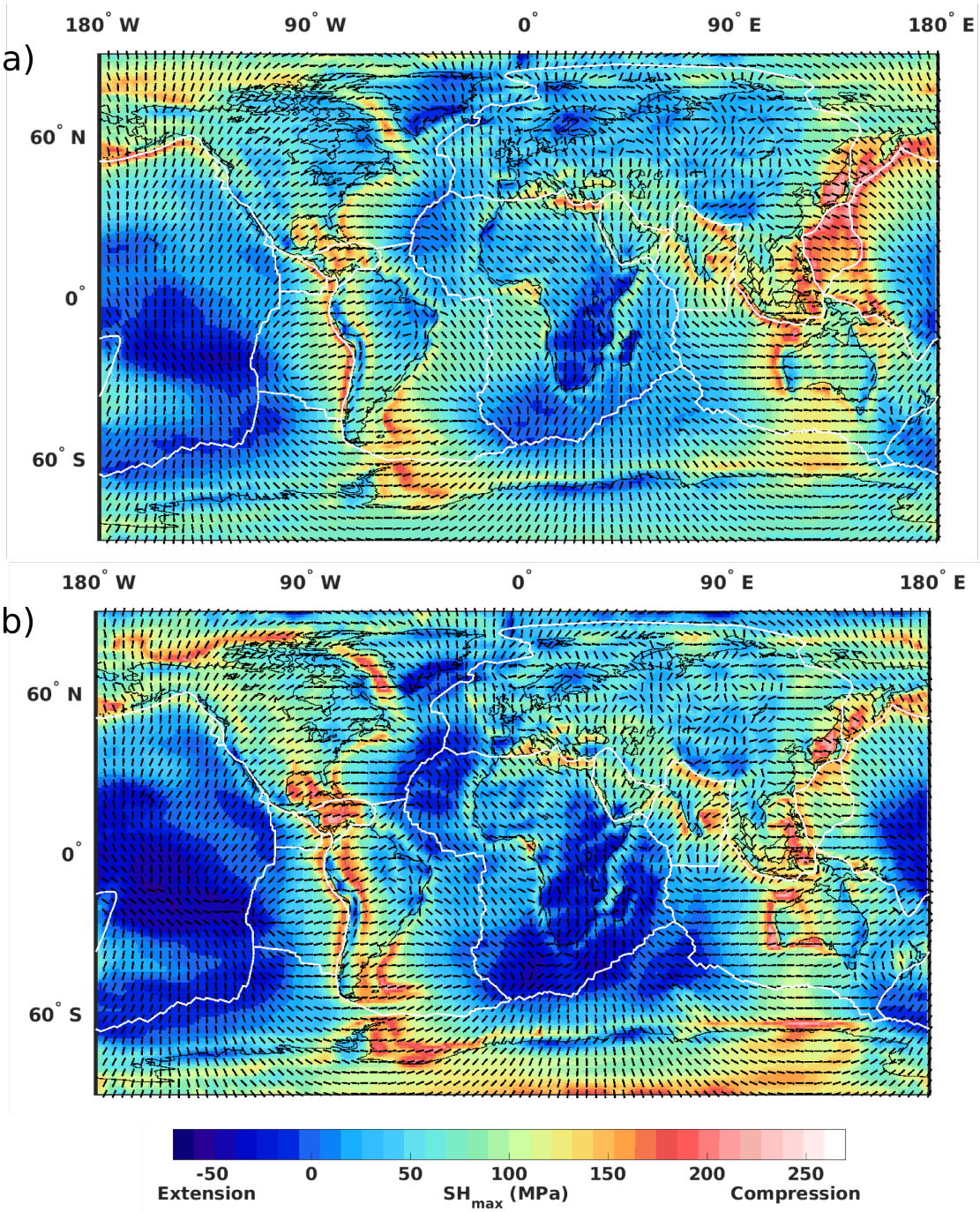

Figure 4: Predictions of the SHmax magnitude and direction from combined contributions due to lower mantle flow and upper mantle from a) TM1 with crust model and b) TM2 with crust model.

Ref 8:
For the stress comparisons, I mention below that Fig. 8a is not necessary. Also Figures 10 and 11 could probably be combined.

AU: The original Figure 8a has been removed, since it's readily available from the World Stress Map repository; so this allowed us to increase the size of the remaining two figures. The regional comparisons have also been combined into one figure, and this is included and further discussed to show how the choice of the upper mantle structure (how well the data source is constrained) influences the model fit to the

WSM2016. AU: Hence, we have excluded Figure 8a and enlarged Figures 8b and 8c (now Figures 5a and 5b) as shown below:

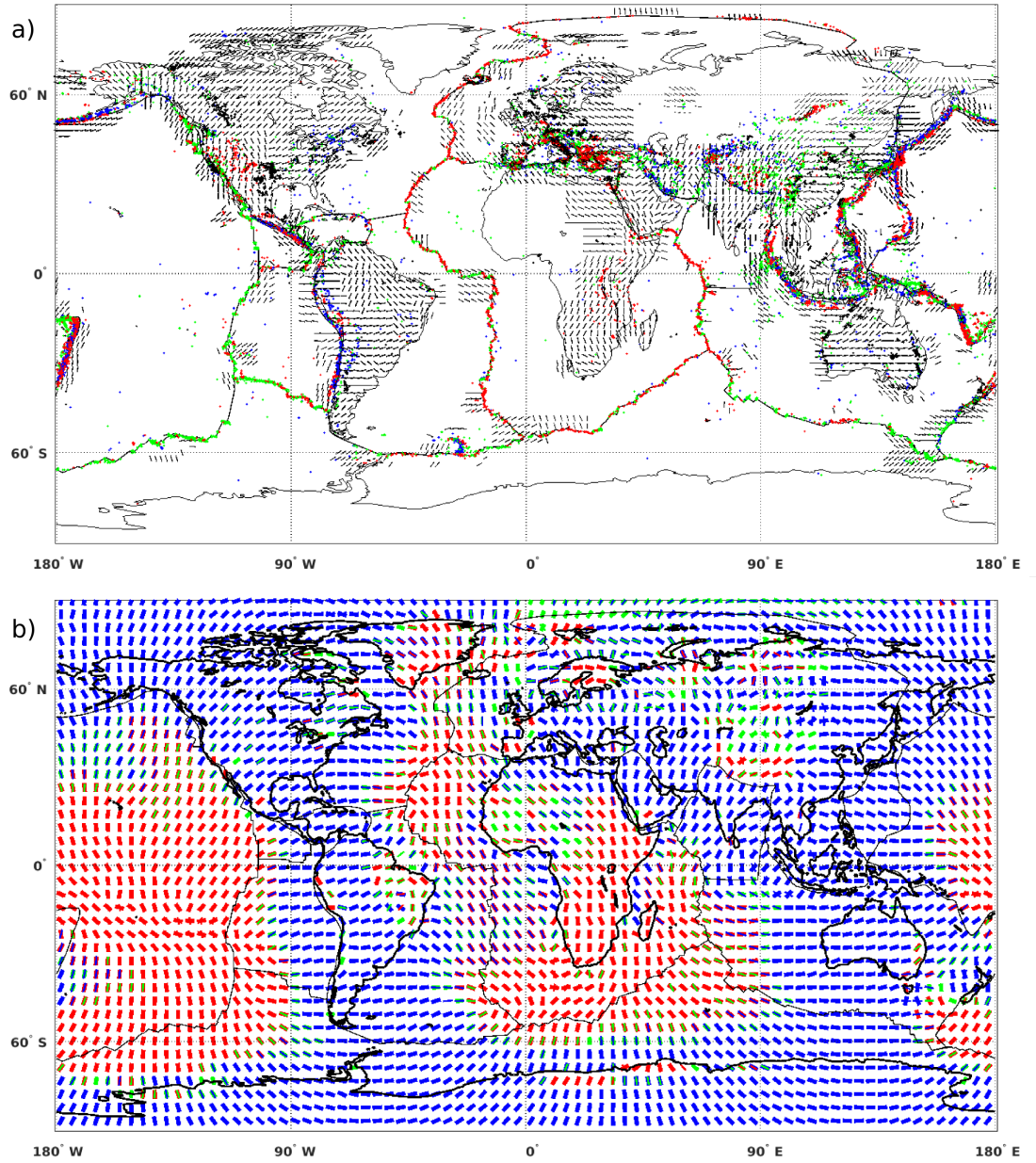

Figure 5: Interpolated World stress map 2016 (Heidbach et al., 2016), data on a grid of 2.5° x 2.5°, using only stress orientation with a constant search radius 270 km, and (b) predicted SHmax orientation and regime from total stress contribution with TM1 (plotted in thin bars) over TM2 (thick bars) upper mantle thermal structures. Colors of dots (a) and bars (b) indicate observed or predicted stress regime with red for normal faults or tensile stress, blue for thrust faults or compressive stress, and green for strike-slip faults or intermediate stress (one principal horizontal stress positive, one negative)

We have combined Figures 10 and 11 as shown below at response to Ref 23.

Ref 9:
Figures 7ab and 12cd both show dynamic topography for models TM1 and TM2, the only difference being that the effect of seafloor age is removed from 12cd. I think that it is appropriate to only use Figs. 12cd and omit 7ab, because the models 12cd are compared to the "observation" models 12ab.

AU: We would like to keep the modeled dynamic topography and the resulting stress field shown in Figure 7 (now Figure 8) to support our discussion on the wide amplitude variations in the modeled dynamic topography due to the isostatic effect of the sea floor cooling, which does not translate into significant variations in stress pattern and also in the scenarios where crustal structure is not considered in continents.

Ref 10:
Figure 13 – I am a little unsure how the amplitudes of spherical harmonic degrees are compared for only parts of the globe (continents or oceans). The spherical harmonics are globally-defined, so does it make sense to compare the spherical harmonic components over the oceans-only or continents-only? How is the rest of the world considered when the spherical harmonic components of the rest of the world are defined? I wonder if it might be better to just do the comparison for the whole globe and avoid this problem?

AU: We have included a discussion of this issue in the manuscript. We assigned the global mean value in continents when computing the ratio for oceans and vice versa. When the same exercise is done with zeros in continents to estimate the oceans ratio and vice versa, there is no change in the shape of the curves but rather, a shift in the vertical axis. To understand the significance of regional features, the contribution of each region at different wavelengths is of particular importance here, but the approach of global ratio or amplitude spectrum for continents and oceans together is not easily distinguishable. With this approach we show that the dominant contribution in the ocean spectrum is between spherical harmonics degrees 1 to 2 with less variability at higher spherical harmonics. However, in continents, we see a wider variability at higher spherical harmonic higher (up to degree 15), mainly coming from cratons, which will guide the corrections for chemical depletion in continental regions.

Ref 11:
Figure 14 – perhaps could be added as an alternative predictive model to Fig. 12?

AU: Done

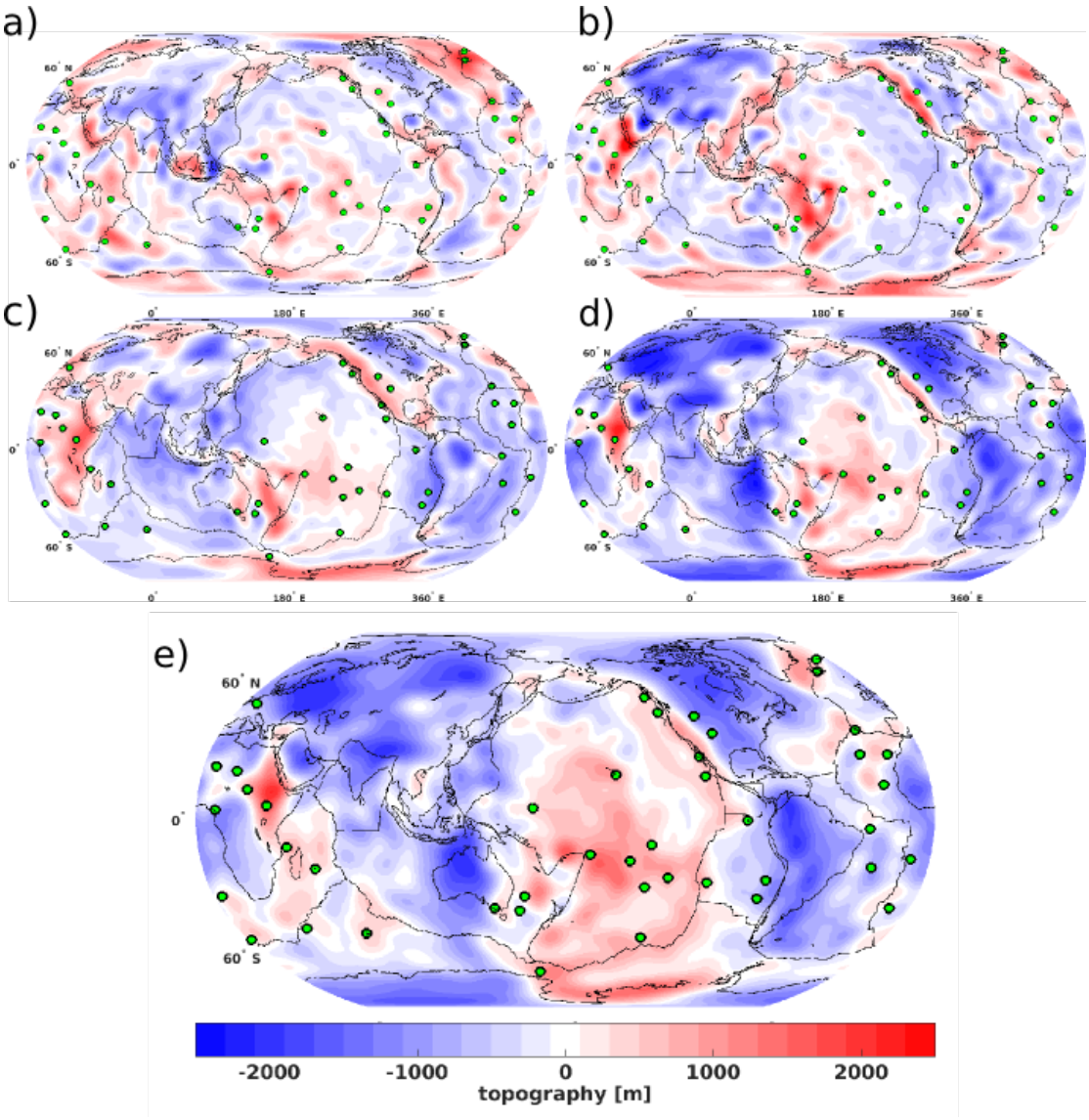

Figure 9: Comparing a) the in-situ observed residual topography from Hoggard et al., (2016), and b) the residual topography based on the CRUST 1.0 from Steinberger, (2016) with modeled dynamic topography using TM1 (c) and TM2 (d) upper mantle thermal density structures with the effect of the sea floor cooling with age removed. Green dots with black circles around show locations of major hotspots

Specific points:

Ref 12:
Title – I think the word "the" should be added before "lithospheric stress field"
AU: The revised title now reads

"Effects of upper mantle heterogeneities on the lithospheric stress field and dynamic topography"

Ref 13: Page 1 – the statements on lines 7-8 and 9-11 basically say the same thing – I think this sort of repetition is not needed in the abstract

AU: The statement spanning lines 9-11 has been removed and an additional revised statement below included:

Ref 14: Page 1, line 12 – stating that a correlation has a value of 0.51 doesn't mean too much to a reader – is this correlation good or poor?
AU: The revised statement reads:

…..giving a good correlation of 0.51 in continents….

Ref 15: P1, L13 – it is not the lithospheric stresses that are being improved, it is the model fit to them.
AU: We have reformulated the statement as:

"……fit between the WSM2016 and the resulting lithosphere stresses."

Ref 16: P1, L15 – the difference in angular misfits reported here (18.3 vs 19.9 deg) doesn't seem very significant – I'm not sure that it is useful to include this information Abstract – generally, it would be good to close the abstract with an overall general statement about what the reader should take away from this study. Currently the abstract doesn't do this.
AU: We revised the abstract to include the statements below:

"Our findings show the disparity of the contributions coming from the shallow and deep mantle dynamic forces to lithosphere stress field and dynamic topography."….

Ref 17: P2, L 27 – this paragraph starts "At longer wavelengths," which seems to differentiate it from the previous paragraph. But both paragraphs are about long wavelengths. It would be better to distinguish this paragraph by stating out the onset that it deals with dynamic topography.

AU: We agree that there is a need to highlight the contrast between the two paragraphs at Lines 15 and 27 regarding the lithosphere stress field and topography. Nonetheless, we briefly discussed the crustal contribution at short wavelengths to the stress field at the end of the former paragraph (Lines 15-26). The revised opening of the later paragraph (Line 27) reads:

"Likewise, the long wavelength signal of topography is related to the vertical component of the stress field tensor originating from the thermal convection of the mantle rocks (Pekeris, 1935; Steinberger et al., 2001)"

Ref 18: P3, L 27 – Here the Bird (2003) approach is described as using the fit to the observed plate motions – this needs a clearer explanation because it contradicts the statement at the onset of the paragraph stating that Bird (2003) was one of two approaches used to fit the stress field (not the plate velocity field).

AU: There seems to be confusion here with regards to our reference to Bird (2003) and Bird et al. (2008). We used the digital model of plate boundaries to predefine our modeling plate boundaries of Bird (2003) to predefine our modeling plate boundaries in the setup as mentioned in the appendix.

With regards to Bird et al. (2008), their study estimates lithosphere stress field, strain rate, plate velocity and seismic anisotropy, using constraints from boundary conditions, variable crust and lithosphere thicknesses, nonlinear rheology and the fit between the modeled and observed plate velocities, by disregarding the effect of deep mantle flow. This approach seemingly works well compared to other studies that have considered the contribution from the deep mantle in addition (Ghosh and Holt, 2012;

Steinberger et al., 2001; Lithgow-Bertelloni and Guynn, 2004). We revised the sentence as below:

"On the other hand, Bird et al. (2008) have estimated the lithospheric stress from a model that disregards the mantle flow contribution and used the fit between the modeled and observed plate velocities as a sole criterion"

Ref 19: P4, L 5 – The paragraph that starts on this line gives many details of the calculations and what was found by them, but these details don't seem necessary for the introduction, and they obscure the description of the main point of what the paper is trying to accomplish.

AU: We agree with this suggestion, since most of these statements are already mentioned in the method and result sections that follow. We have reformulated this part of the introduction as shown below:

"To date, two distinct approaches have been adopted to study the origin of the lithospheric stress, and each has given a relatively good fit to the observed stress field. On the one hand, Bird et al. (2008) have estimated the lithospheric stress from a model that disregards the mantle flow contribution and used the fit between the modeled and the observed plate velocities as a sole criterion}. On the other hand, Ghosh et al., (2013), Ghosh ad Holt (2012), Lithgow-Bertelloni and Guynn (2004), Steinberger et al., (2001) and Wang et al., (2015) have aimed at assessing the influence of the mantle flow on the lithospheric stress field and have shown that the bulk mantle flow explains a large part (about 80-90 %) of the stress field accumulated in the lithosphere Steinberger et al., (2001), in both magnitude and the most compressive horizontal direction. The aim of the present study is to evaluate the contribution of the upper mantle density and viscosity heterogeneities above the transition zone to the observed spatial stress regimes of the lithosphere (Heidbach et al., 2016), while testing different approaches and data sets used to describe the thermal and rheological structure of the upper mantle and the crust. We use a 3D global lithosphere-asthenosphere finite element model (Popov and Sobolev 2008; Sobolev et al., 2009) with visco-elasto-plastic rheology, which is coupled to a spectral model of mantle flow (Hager and O'Connell, 1981) at 300 km depth. Deriving all force contributions from a single calculation resolves any inconsistency that might arise from treating individual force contributions to the stress field separately, as has been done in earlier studies (Bird et al, 2008; Steinberger et al 2001; Lithgow-Bertelloni and Guynn, 2004; Ghosh et al., 2008; Naliboff et al., 2012; Ghosh et al., 2013; Wang et al., 2015). As part of this work, we further estimate dynamic topography and correlate our results with two different residual topography models. One is based on seismic surveys of the ocean floor used to correct for shallow contributions to topography and free-air gravity anomalies on continents Hoggard et al., (2016). The second model is taken from Steinberger (2016) and is based on actual topography corrected for crustal thickness and density from CRUST1.0 (Laske et al., 2013). "

Ref 20: P6, L 5 – Why does the model have to be run for 0.5 Myr? It seems to me that the authors are basically doing an instantaneous flow calculation, and so advancing in time is not necessary. If the 5 kyr time-steps serve as a way to iterate on the consistency between the upper and lower models, then the authors should state this (and there would be no need to advance the model for any particular length of time).

AU: The study results are compared with present-day observables (WSM2016 and residual topography), which is why we have restricted our calculations to half a million of years.

*Correction->There is also a typographical error in our time-step; it's 50 kyr not 5kyr.

Yes, you are right that using 50-kyr time-steps allows us to track our iterations between the two-coupled components for consistency. As we have mentioned in the manuscript (Page 6, Line 30) this is done by comparing the norms of the velocities and tractions from two successive iterations.

Ref 21: P8, L24 – the authors call a correlation of 0.82 as "relatively low" but it doesn't seem too much different than the correlation of 0.85, which was viewed more favorably earlier. Fig. 3a – there is no scale bar for this figure to show how colors relate to geoid height.

AU: We report this correlation difference for the modeled geoid with and without lateral viscosity variations (LVVs) in the top 300 km to highlight, how the global correlation up to spherical harmonic degree 31 alone does not show the improvement in the fit to the observed geoid. However, looking at the degree-by-degree correlation and amplitude spectrum gives us more information about contribution of lateral viscosity in the top 300 km, as shown in the Figure 2R below. This support the conclusion of by Čadek and Fleitout (2003) about the importance of LVVs in the top 300 km. The figure below is included the supplementary of Osei Tutu et al. (2018). Also we have corrected the geoid figure by including the colorbar shown above in Figure 2 response to Ref 4.

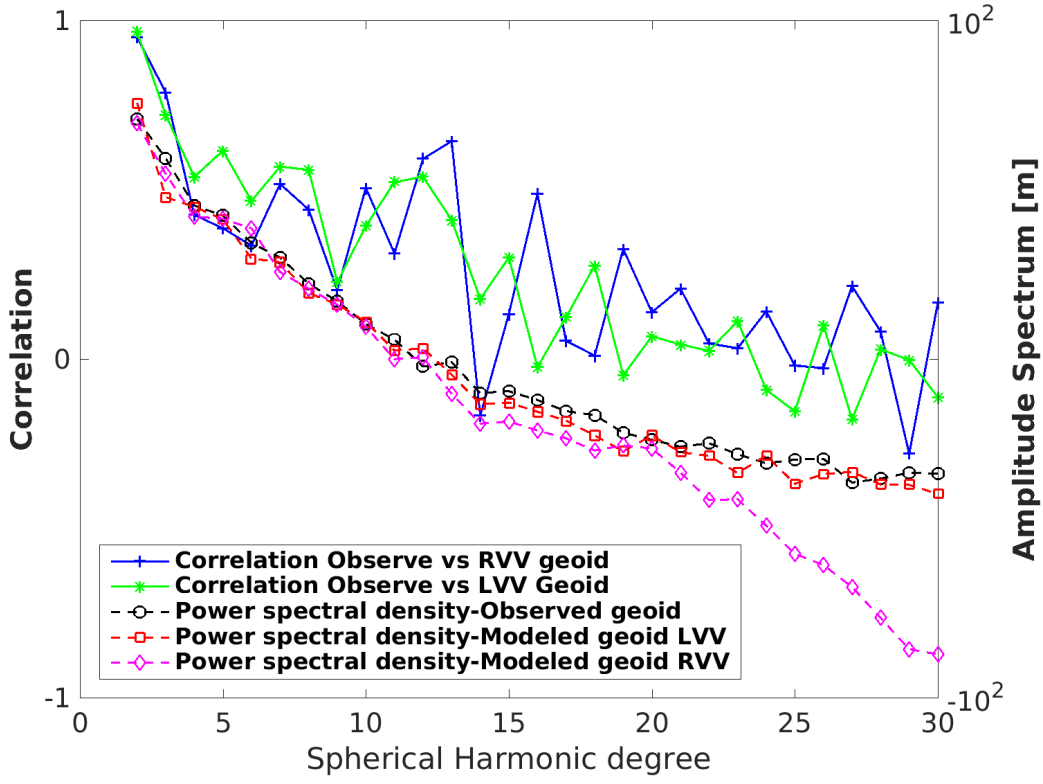

Figure 2R: Estimates of correlation and amplitude spectrum of modeled and observed geoid for spherical harmonic degrees l =1to 30

Ref 23: P10, L15 – many of the setup details in this section seem to be repeated from previous sections.

AU: We revised the beginning of the paragraph as below to avoid the repetition of the model set up:

"We start with examining separate contributions of the mantle heterogeneities below 300 km (deep Earth setup) and above (shallow Earth setup) to the global lithospheric stress field and topography. To calculate the contribution of the lower domain, we use a constant lithosphere thickness (100 km) and density (3.27 kg/m^3), with a configuration of the mantle below similar to that used to derive the geoid anomaly, plate motions and the shear tractions in Figure 3a-c"

Figure 8a – I think this figure is unnecessary, as the data of the WSM have been published elsewhere and are repeated in the interpolation shown in Fig. 8b. Getting rid of Fig. 8a would allow Figures 8b and 8c to be larger, which make the figures easier to see and compare.

AU: Done in above at figure at response to Ref 8.

Ref 22: P 17 – Some of the discussion on this page about the comparison of the modeled and predicted stresses is more easily discussed in section 3.5.1, which refers to Fig. 9. I suggest condensing the second paragraph on page 9 and combining it into section 3.5.1, which would shorten this section on the overall comparison.

AU: We have combined the second paragraph of section 3.5 and combined with section 3.5.1 and the regional comparison, which is highlighted in red in the tracking manuscript and shown here below:

"See the attached tracked manuscript below"

Ref 23: Figures 10 and 11 – Most of the information in these figures is already in Fig. 9, so perhaps these regional details are not necessary? I also think that the discussion of these figures could be shortened.

AU: These regional detail comparisons are considered in order to discuss the implications of the continental thermal structures used, their strengths and weaknesses and influence on the model stress field on regional basis. The figures of the angular misfit for Western Europe and Australia are discussed in detail to show the impact of the well-constrained thermal structures in these regions on the lithosphere stress field and the fit to the observed stress field. We as well point out how treating slabs also influence the fit in subduction regions, as given in the revised manuscript and the accompanying tracking manuscript.

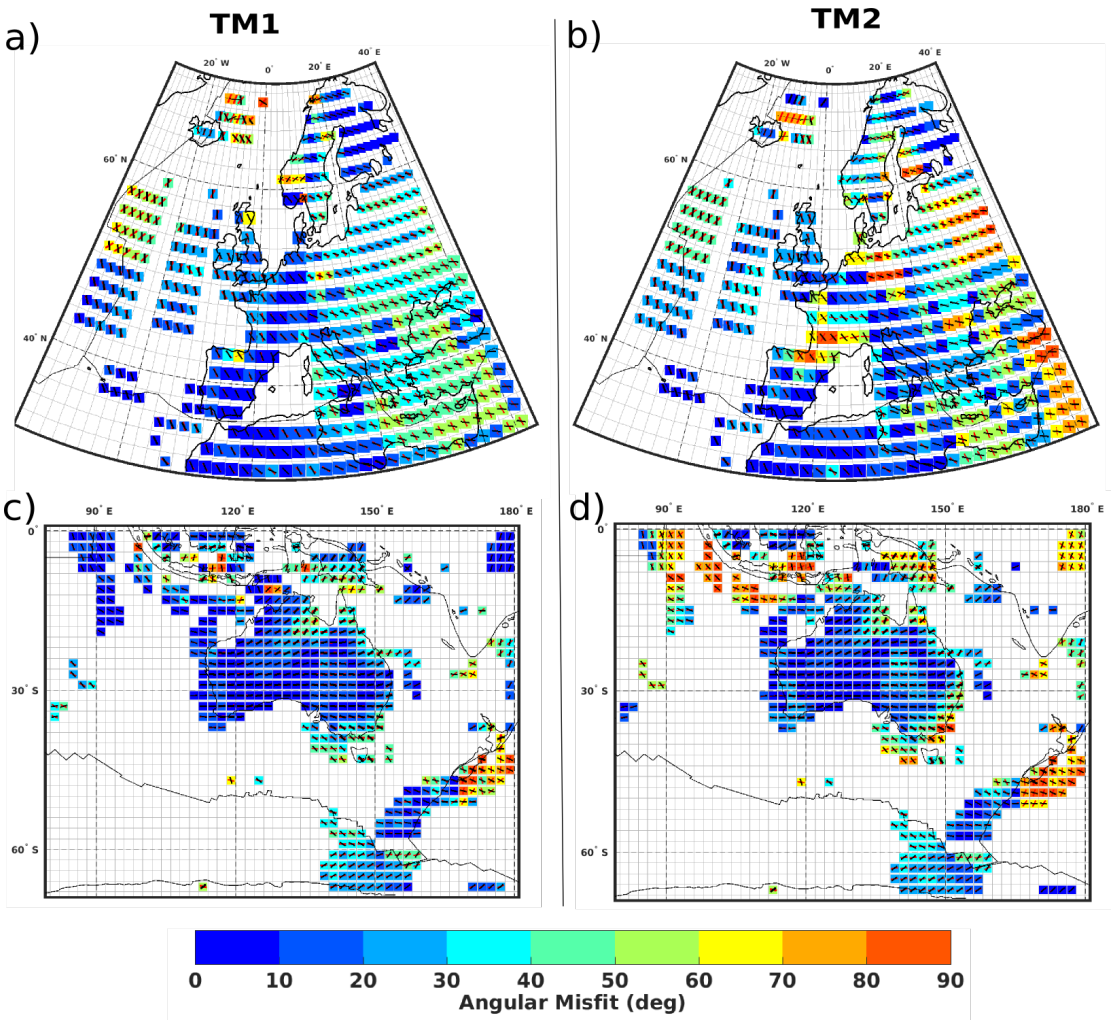

Figure 7: Regional comparison of the angular misfit in Europe (a and b) and Australia (c and d) between the observed and modeled total stresses with TM1 (a-c) and TM2 (d-f). Red bars denote modeled orientations versus black bars showing the smoothed observed stress field (WSM2016).

Ref 24: Fig. 13 – the background grid in this figure is 0.5 harmonic degrees, which is unnecessary. It would make more sense to use 1.0 degree for the background grid (since half degrees are unphysical).

AU: We have re-plotted figure 13, now as figure 11, using background grid interval of spherical harmonic degree 1 as shown below.

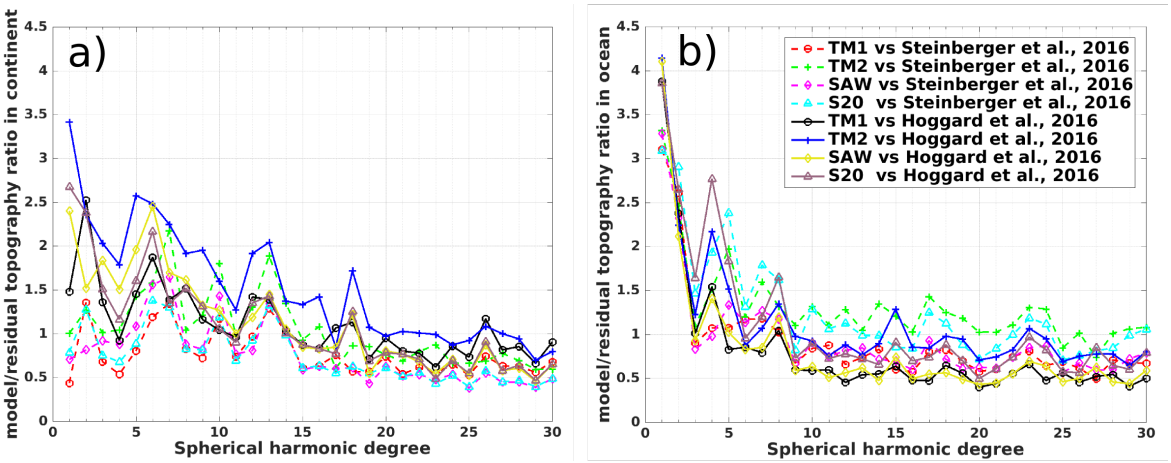

Figure 10: Ratio of modeled dynamic topography from TM1 and TM2 for (a) continents and (b) oceanic regions with observations based residual topography from Steinberger (2016) and (Hoggard et al., (2016)

References

Čadek, O. and L. Fleitout. 2003. "Effect of Lateral Viscosity Variations in the Top 300 Km on the Geoid and Dynamic Topography." *Geophysical Journal International* 152(3):566–80. Retrieved May 10, 2016 (http://doi.wiley.com/10.1046/j.1365-246X.2003.01859.x).

Hoggard, M. J., N. White, and D. Al-Attar. 2016. "Global Dynamic Topography Observations Reveal Limited Influence of Large-Scale Mantle Flow." *Nature Geoscience*. Retrieved May 25, 2016 (http://www.nature.com/doifinder/10.1038/ngeo2709).

Osei Tutu, A., S. V Sobolev, B. Steinberger, A. A. Popov, and I. Rogozhina. 2018. "Evaluating the Influence of Plate Boundary Friction and Mantle Viscosity on Plate Velocities." *Geochemistry, Geophysics, Geosystems* n/a-n/a. Retrieved (http://dx.doi.org/10.1002/2017GC007112).

Steinberger, Bernhard. 2016. "Topography Caused by Mantle Density Variations: Observation-Based Estimates and Models Derived from Tomography and Lithosphere Thickness." *Geophysical Journal International* 205(1):604–21. Retrieved May 19, 2016 (http://gji.oxfordjournals.org/lookup/doi/10.1093/gji/ggw040).

Effects of upper mantle heterogeneities on *the* lithospheric stress field and dynamic topography

Anthony Osei Tutu[1,2], Bernhard Steinberger[1,3], Stephan V. Sobolev[1,2], Irina Rogozhina[4,1], and Anton A. Popov[5]

[1]Section 2.5 Geodynamic modelling, GFZ German Research Centre for Geosciences, Potsdam, Germany
[2]Institute of Earth and Environmental Science, University of Potsdam, Potsdam, Germany.
[3]Centre for Earth Evolution and Dynamics, University of Oslo, Oslo, Norway.
[4]MARUM Centre for Marine Environmental Sciences, University of Bremen, Bremen, Germany.
[5]Institute of Geosciences, Johann Gutenberg University, Mainz, Germany.

Correspondence to: Anthony Osei Tutu (oseitutu@gfz-potsdam.de)

Abstract. The orientation and tectonic regime of the observed crustal/lithospheric stress field contribute to our knowledge of different deformation processes occurring within the Earth's crust and lithosphere. In this study, we analyze the influence of the thermal and density structure of the upper mantle on the lithospheric stress field and topography. We use a 3D lithosphere-asthenosphere numerical model with power-law rheology, coupled to a spectral mantle flow code at 300 km depth. Our results are validated against the World Stress Map 2016 *(WSM2016)* and the observation-based residual topography. We derive the upper mantle thermal structure from either a heat flow model combined with a sea floor age model (TM1) or a global S-wave velocity model (TM2). We show that lateral density heterogeneities in the upper 300 km have a limited influence on the modeled horizontal stress field as opposed to the resulting dynamic topography that appears more sensitive to such heterogeneities. ~~There is hardly any difference between the stress orientation patterns predicted with and without consideration of the heterogeneities in the upper mantle density structure across North America, Australia, and North Africa~~. In contrast, we find that the dynamic topography is to a greater extent controlled by the upper mantle density structure. After correction for the chemical depletion of continents, the TM2 model leads to a much better fit with the observed residual topography giving a *good* correlation of 0.51 in continents, but this correction leads to no significant *improvement of the fit between the WSM2016 and the resulting lithosphere stresses*. In continental regions with abundant heat flow data such as, for instance, Western Europe, TM1 results in relatively a small angular misfits of 18.30° between the modeled and observation-based stress field compared to 19.90° resulting from modeled lithosphere stress with s-wave based model TM2. *Our findings show the disparity of the contributions coming from the shallow and deep mantle dynamic forces to lithosphere stress field and dynamic topography*

1 Introduction

The stresses building up in the rigid outermost layer of the Earth are the result of both shallow and deep geological processes. Lithosphere dynamics are defined by a combination of plastic, elastic and viscous flow properties of the lithospheric material (Burov, 2011; Tesauro et al., 2012), while the evolution of the sub-lithospheric mantle is predominantly driven by viscous flow (Davies, 1977; Forte and Mitrovica, 2001; Steinberger and Calderwood, 2006). ~~This is evident from surface expressions of different deformation processes around the globe, such as for example the ongoing crustal deformation processes that formed the Tibetan Plateau due to the continental collision of the Indian and Eurasian Plates (van Hinsbergen et al., 2011) or the rifting of the African Plate induced by its interaction with the Afar plume head (Ebinger and Sleep, 1998).~~ It has been shown that shallow processes influence both the magnitude and orientation of the lithospheric stresses. Among such processes the most important are slab pull, ridge push, trench *friction* and continental collision (deformation) (Reynolds et al., 2002) as well as cratonic root resistance (Naliboff et al., 2012). Also, gravitational effects due to lateral density heterogeneities in the lithosphere and tractions from the mantle flow at the base of the moving plates play an important role. Superposition of different tectonic forces creates dissimilar orientations and regimes of the lithospheric stress field in different regions, as shown by the World Stress Map project (Bird and Li, 1996; Heidbach and Höhne, 2007; Heidbach et al., 2008, 2016).

Furthermore, on a global scale, the intra-plate stress orientation follows a specific pattern at a longer wavelength due to a large force contribution from the convecting mantle (Steinberger et al., 2001; Lithgow-Bertelloni and Guynn, 2004). This first-order stress pattern (long wavelength) is dynamically supported, as the controlling forces correlate well with the forces driving the plate motion in most continental areas such as North and South Americas and Europe (Solomon et al., 1980; Richardson, 1992; Zoback, 1992). Ghosh and Holt (2012) and Steinberger et al. (2001) used different approaches to show that the contribution of the crust (shallow density structures) to the overall lithospheric stress pattern is rather small compared to that of the mantle buoyancy forces, amounting to ~10 %, except for regions characterized by high altitudes, especially the Tibetan Plateau, where the contribution is larger. In these previous modeling studies, the effect of the crust was determined separately by computing the gravitational potential energy from a crust model, which was subsequently applied as a correction (Steinberger et al., 2001; Ghosh et al., 2013; Ghosh and Holt, 2012). The contribution of the crust with a shallow lithospheric density contrast generates the second-order pattern (mid-to-short wavelength) in the stress field, mostly coming from topography and crustal isostasy (Zoback, 1992; Zoback and Mooney, 2003; Bird et al., 2006).

Likewise,the long-wavelength signal of the topography is related to the vertical component of the stress field tensor originating from the thermal convection of the mantle rocks (Pekeris, 1935; Steinberger et al., 2001). This generates a high dynamic topography in regions of upwelling over the African and Pacific Large Low Shear Velocity Provinces (LLSVP) and low topography above downwelling in the regions of subduction (Hager and O'Connell, 1981; Hager et al., 1985). On the other hand, at a mid-to-short wavelength, topographic features are influenced by processes such as plume-lithosphere interaction (Lithgow-Bertelloni and Silver, 1998; Thoraval et al., 2006; Dannberg and Sobolev, 2015) and small-scale convection in the upper mantle (Marquart and Schmeling, 1989; King and Ritsema, 2000; Hoggard et al., 2016). However, the largest fraction of topography is caused by isostasy due to variations in crustal thickness and density, as well as density variations in the sub-

crustal lithosphere. *Comparatively, the fit between the modeled dynamic and the observational-based residual topographies is lower (Heine et al., 2008; Flament et al., 2012; Steinberger and Calderwood, 2006; Steinberger, 2016; Hoggard et al., 2016), than corresponding fits from mantle flow simulations of other geophysical processes. For example, the modeled and the observed geoid show relatively higher correlation (Čadek and Fleitout, 2003; Hager et al., 1985; Richards and Hager, 1984) due to a large contribution of the lower mantle but the modeled geoid is sensitive to the choice of the mantle viscosity (Thoraval and Richards, 1997). One of the reasons for the low correlation between modeled and residual topographies is our insufficient knowledge of the petrological properties of the upper mantle (Cammarano et al., 2011), for example in relation to the chemical depletion of cratons in continental regions. Hence, in this study we test in addition to evaluating the influence of thermal-density heterogeneities on lithosphere stress field and topography, we test the impact of applying corrections for the continental depletion on the topography and stress field.*

~~A number of studies (Čadek and Fleitout, 2003; Forte and Mitrovica, 2001; Garcia-Castellanos and Cloetingh, 2011; Ghosh and Holt, 2~~ ~~have presented numerical simulations of different geophysical processes and compared their model results with observations of the lithosphere stress field, dynamic geoid, plate motion velocity and dynamic topography to better understand what processes control these surface observables. For instance, the modeled dynamic geoid typically gives a good correlation with observations, due to a large contribution of the lower mantle (Čadek and Fleitout, 2003; Hager et al., 1985; Richards and Hager, 1984), but is sensitive to the choice of the mantle viscosity (Thoraval and Richards, 1997). However, the correlation between the modeled dynamic and residual topography is typically found to be weak (Heine et al., 2008; Flament et al., 2012; Steinberger and Calderwo~~ ~~The residual topography is here defined as the observed topography corrected for the variations in the crustal and lithosphere thickness and density variations and for subsidence of the sea floor with age. *Also at tectonic-scale topography is influenced by the elastic-b*~~ ~~One of the reasons for dissimilarities between the modeled and observed topography is our insufficient knowledge of the petrological properties of the upper mantle (Cammarano et al., 2011), for example in relation to the chemical depletion of cratons in continental regions. This is further amplified by the uncertainties in the complex rheological and density structure of the upper mantle due to a wide range of thermal regimes associated with cold subducting plates and cratons, hot plumes and small-scale convection cells (Ebinger and Sleep, 1998; Thoraval et al., 2006). Another reason is linked to the deficiencies of the state-of-the-art seismic tomography models that often fail to provide the necessary detail about the density/thermal heterogeneities in the upper mantle. Finally, crustal models (e.g. Laske et al., 2013) used to compute the observation-based residual topography are not well constrained, in particular in oceanic regions~~.

Also, constraining the modeled lithospheric stress with observations is challenging due to previously poor spatial coverage by the World Stress Map data (Zoback, 1992; Lithgow-Bertelloni and Guynn, 2004; Heidbach et al., 2008). An alternative way documented in the literature is to compare the strain rate estimated from the modeled deviatoric stresses (Ghosh et al., 2008) with the Global Strain Rate Map (Kreemer et al., 2003). However, the lithospheric stress in plate interiors (i.e. far from the plate boundaries) is not well constrained with the Global Strain Rate Map. Hence, a gradually increasing coverage of the observed global stress field data serves as a motivation for studies attempting a global comparison of the observed and modeled stress field patterns, including our present study.

To date, two distinct approaches have been adopted to study the origin of the lithospheric stress, and each has given a relatively good fit to the observed stress field. *On the one hand, Bird et al. (2008) have estimated the lithospheric stress from a model that disregards the mantle flow contribution and used the fit between modeled and observed plate velocities as a sole criterion*. On the other hand, Ghosh et al. (2013), Ghosh and Holt (2012), Lithgow-Bertelloni and Guynn (2004), Steinberger et al. (2001) and Wang et al. (2015) have aimed at assessing the influence of mantle flow on the lithospheric stress field and have shown that the bulk mantle flow explains a large part (about 80-90 %) of the stress field accumulated in the lithosphere (Steinberger et al., 2001), in both magnitude and the most compressive horizontal direction. *The aim of the present study is to evaluate the contribution of the upper mantle density and viscosity heterogeneities above the transition zone to the observed spatial stress regimes of the lithosphere (Heidbach et al., 2016), while testing different approaches and data sets used to describe the thermal and rheological structure of the upper mantle and the crust. We use a 3D global lithosphere-asthenosphere finite element model (Popov and Sobolev, 2008; Sobolev, 2009) with visco-elasto-plastic rheology coupled to a spectral model of mantle flow (Hager and O'Connell, 1981) at 300 km depth. Deriving all force contributions from a single calculation resolves any inconsistency that might arise from treating individual force contributions to the stress field separately, as has been done in earlier studies (Bird et al., 2008; Steinberger et al., 2001; Lithgow-Bertelloni and Guynn, 2004; Ghosh et al., 2008; Naliboff et al., 2012; Ghosh et al., 2013; Wang et al., 2015). As part of this work, we further estimate dynamic topography and correlate our results with two different residual topography models. One is based on seismic surveys of the ocean floor used to correct for shallow contributions to topography and free-air gravity anomalies on continents (Hoggard et al., 2016). The second model is taken from Steinberger (2016) and is based on actual topography corrected for crustal thickness and density from CRUST1.0 (Laske et al., 2013). Both models are also corrected for subsidence of sea floor with age*.

~~In this study, a 3D global lithosphere-asthenosphere finite element model (Popov and Sobolev, 2008) with visco-elasto-plastic rheology is coupled to a spectral model of mantle flow (Hager and O'Connell, 1981) at 300 km depth. As part of this work, we estimate dynamic topography and correlate our results with two different residual topography models. One is based on seismic surveys of the ocean floor used to correct for shallow contributions to topography and free-air gravity anomalies on continents (Hoggard et al., 2016). The second model is taken from Steinberger (2016) and is based on actual topography corrected for crustal thickness and density from CRUST1.0 (Laske et al., 2013). Both models are also corrected for subsidence of sea floor with age. To derive our stress model we have combined CRUST 1.0 with the thickness and thermal structure of the lithosphere estimated by Artemieva (2006) in continents, and a half-space cooling model of the ocean floor with age (Müller et al., 2008). This is an improvement compared to much simpler representations of the upper mantle structure in previous studies using a thin-sheet/shell approximation (Steinberger et al., 2001; Lithgow-Bertelloni and Guynn, 2004; Ghosh and Holt, 2012; Ghosh et al., 2013; also account for the presence of slab locations and their corresponding impact on the upper mantle temperature based on Steinberger (2000). Stresses induced by regional and global variations in the crustal and lithospheric structures are of the order of 100 MPa in magnitude across strongly uplifted continental areas (Artyushkov, 1973). It is therefore clear that including a variable lithosphere and crustal thickness in calculations is preferable over the use of the thin-sheet/shell method (Steinberger et al., 2001; B In addition we have used a seismic velocity model to derive an alternative model of the lithosphere thickness and thermal density structure to counterpose the results from two simulations. While studying the impacts of the shallow (upper mantle)~~

~~thermal and density anomalies and lateral variations in the rheological properties on the present-day dynamic topography and lithospheric stress state, we also attempt to quantify the uncertainties in the thermal structure of the upper mantle and their potential effects on the dynamic topography. As part of this analysis, we test the ability of our new 3D thermo-mechanical model of the lithosphere and asthenosphere coupled to the mantle flow to reproduce the spatial pattern of the topographic anomalies and use it to separate out the effects of the chemical depletion in cratonic regions on the dynamic topography and lithospheric stress field~~.

2 Method

2.1 Model description

Our global numerical model of the Earth interior consists of the particle-in-cell finite element model SLIM3D (Popov and Sobolev, 2008) within the top 300 km, which solves coupled momentum and energy equations with a semi-Lagrangian Eulerian grid with a free top boundary condition and a Winkler dynamic bottom boundary condition, which is coupled to a spectral mantle flow code (Hager and O'Connell, 1981) to account for the deep mantle contributions. There is no material exchange across the coupling interface, but the continuity of tractions and velocities is ensured through the Newton-Raphson iteration method. Figure 1(c) shows a sectional schematic representation of the coupled numerical model with depth-dependent layered mantle viscosity structure (Figure 1b) and seismic velocity-to-density scaling profile of Steinberger and Calderwood (2006) (Figure 1a), which are only considered below the depth of 300 km. The top thermo-mechanical component (SLIM3D) has been used in a wide range of 2D and 3D regional numerical studies of crustal and lithospheric deformations (Popov and Sobolev, 2008; Brune et al., 2012, 2014, 2016; Popov et al., 2012; Quinteros and Sobolev, 2013) with different spatial and temporal resolutions, but the coupled code is used here and in Osei Tutu et al. (2018) for the first time. In this 3D global study, we distinguish three material layers (phases) within the top component (SLIM3D), the crustal layer, the lithosphere and the sub-lithospheric mantle layers, in order to account for the stress and temperature-dependent rheology in the presence of major continental keels and the uppermost part of the subducted lithospheric plates. The visco-elasto-plastic rheology is described in detail by Popov and Sobolev (2008), with specific modeling parameters given in Osei Tutu et al. (2018) and here in the appendix.

This study complements our previous study (Osei Tutu et al., 2018) about the influence of plastic yielding at plate boundaries on plate velocities in a no-net-rotation reference frame and on lithospheric net rotation. A forward model is run for half a million years with a time step of 50 kyr, and at each time step tractions in the lower mantle due to density heterogeneities are computed using the spectral mantle code and then passed across the coupling dynamic boundary to the top component SLIM3D. Within the upper domain (SLIM3D), the flow velocities are then computed and passed back across the coupling boundary as an upper boundary condition to the spectral mantle code, with the method convergence estimated by comparing the velocity and traction norms of two successive iterations. Within the upper mantle, our crustal rheology is taken from Wilks (1990) and below the crust we have considered dry and wet olivine parameters in the lithosphere and sub-lithospheric mantle layers, respectively, modified after the axial compression experiments of Hirth and Kohlstedt (2004) (shown in the appendix, Table A1. Adopted from Osei Tutu et al. (2018) for studying the influence of both the driving and resisting forces that generate global plate velocities and lithospheric plate net rotation).

2.2 Thermal and density structures of the upper and lower mantle

We assign densities of the uppermost layers according to the crustal model CRUST1.0 (Laske et al., 2013). Underneath, we separately consider the layers below and above the interface between the two codes placed at a depth of 300 km to differentiate between the deep and shallow signals. Here the topographic signal induced by the layers below 300 km is assumed to be due

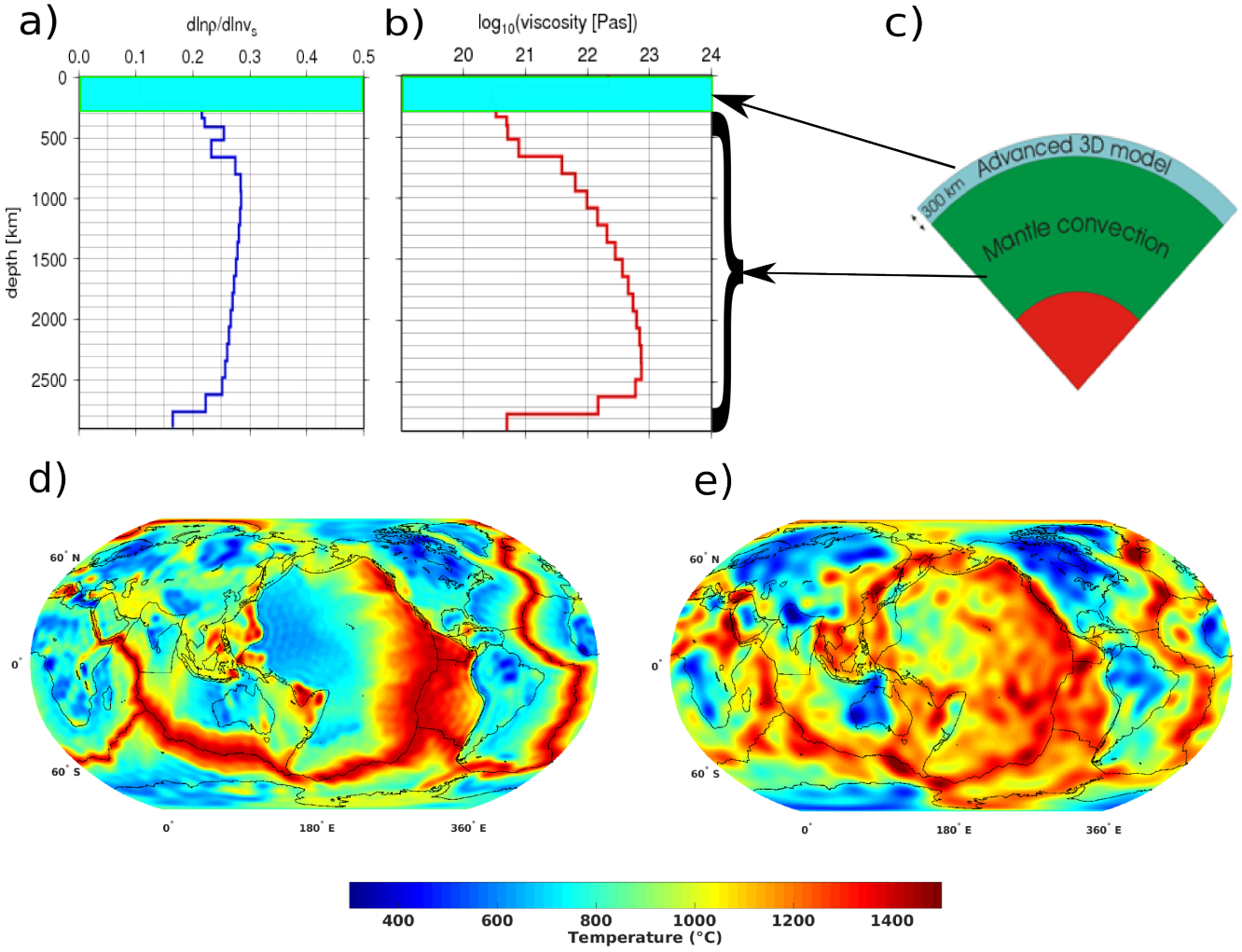

Figure 1. *Adopted from Osei Tutu et al. (2018) (a) Depth-dependent scaling profile of S-wave velocity to density; (b) radial mantle viscosity structure (Steinberger and Calderwood, 2006) and (c) a schematic diagram of the numerical method that couples the 3D-lithosphere-asthenosphere code SLIM3D (Popov and Sobolev, 2008) to a lower mantle spectral flow code (Hager and O'Connell, 1981) at a depth of 300 km. The 3D thermal structure of the upper mantle at a depth of 80 km is shown for two reference thermal models adopted in this study. d) TM1, a heat flow-based thermal structure inferred from the TC1 model of Artemieva (2006) in the continents and the sea floor age model of Müller et al. (2008) in the oceanic areas. e) TM2, the thermal structure of the upper mantle inferred from the S-wave tomography model SL2013sv of Schaeffer and Lebedev (2013). The "ring ing" visible in tpanel (d) is a side effect introduced by smoothing sharp boundaries with a spherical harmonic expansion.*

to convection in the viscous mantle, although cold rigid subducting slabs (Zhong and Davies, 1999; Faccenna et al., 2007) and possibly also the deepest cratonic roots (Conrad and Lithgow-Bertelloni, 2006) extend deeper than 300 km. We use a 3D density structure inferred from the hybrid seismic tomography model of Becker and Boschi (2002) and apply a velocity-to-density conversion profile (Figure 1a) for the lower mantle buoyancy. In the upper mantle we test two different models for the representation of the upper mantle thermal and density structures, namely TM1 (Figure 1d) and TM2 (Figure 1e). *TM1 is based on the 3D thermal structure TC1 model (Artemieva, 2006) across continents. This is combined with the a 3D thermal structure inferred from sea floor age (Müller et al., 2008) for the mantle under oceanic regions. We use a half-space cooling model to infer the temperature T_{ocean} as a function of age and depth according to:*

$$\mathrm{T}_{ocean}(z,\tau) = \mathrm{T}_s + (\mathrm{T}_m - \mathrm{T}_s)\, erf\left(\frac{z}{2\sqrt{k\tau}}\right) \tag{1}$$

where $k = 8 \cdot 10^{-7} m^2 s^{-1}$ is the thermal diffusivity, τ is the age of the oceanic lithosphere, T_s is the reference surface temperature, T_m is the reference mantle temperature, with z being the depth beneath the Earth's surface. In regions of continental shelf, where there is neither age grid nor heat flow data, we interpolated the resulting thermal structures surrounding these regions while in Iceland the TC1 model was assigned. The second model of the upper mantle thermal structure (TM2) is inferred from the seismic tomography model SL2013sv (Schaeffer and Lebedev, 2013). We have chosen this model because of its detailed representation of the upper mantle heterogeneities, which has been shown by Steinberger (2016) to allow a better prediction of the dynamic topography than previous models. This makes it a good candidate for comparison with the model results obtained using TM1, and for a regional investigation of the upper mantle contribution to the lithospheric stresses and topography. Here we convert seismic velocity anomalies δV_s into thermal anomalies ΔT within the upper mantle according to the relation:

$$\Delta T = \frac{\left(\frac{\delta V_s}{V_s(z)}\right)}{\left(\frac{\partial \ln V_s}{\partial T}\right)_P}, \tag{2}$$

where the subscript P stands for a partial derivative at constant pressure (i.e. depth) based on Steinberger (2007). As a first step, we do not correct for the effect of the chemical depletion in cratons in order to evaluate its influence on the modeled lithospheric stress field and topography. In addition and for comparison purposes, we introduce two other thermal models based on two different seismic tomography models SAW24B16 (Mégnin and Romanowicz, 2000) and S20RTS (Ritsema et al., 2011) to evaluate their performance relative to our reference seismic tomography model SL2013sv (Schaeffer and Lebedev, 2013) (Figure 1e). In our model setup, we define the reference crustal, lithospheric and asthenospheric densities (Table A1) and account for lateral density variations linked to thermal anomalies (Figure 1) using the relation:

$$\rho(\Delta T) = \rho_{ref}\left[1 - \alpha \Delta T + \frac{P}{K}\right], \tag{3}$$

where ρ_{ref} denotes the reference density at a reference temperature of 20°C and zero pressure, α denotes the thermal expansion coefficient chosen to be 2.7 $\times 10^{-5}\mathrm{K}^{-1}$ in the crustal layer and $3 \times 10^{-5}\mathrm{K}^{-1}$ within the lithospheric and asthenospheric mantle and K is the bulk modulus (Table A1).

3 Results and Discussion

3.1 Average creep viscosities and corresponding basal tractions

We follow the study of Osei Tutu et al. (2018) with estimates of global dynamic geoid and plate motion velocity to test whether our prescribed lateral viscosity variations within the upper mantle yield realistic results. Together with the resulting shear tractions at depth 300 km, which are generating stresses in the lithosphere, results are shown in Figure 2(a-c) ~~(see the slice in figure 2(d) for illustration)~~ . We compared our predicted geoid (Figure 2a) calculated with a 3-D viscosity structure within the upper 300 km to the observation-based GRACE model (Reigber et al., 2004) (see Supplementary Information Figure S2a) yielding a correlation of 0.85 at spherical harmonic degree *l = 1-31*. We also compared it to the geoid estimate from the simulation using a layered/radial viscosity structure (Steinberger and Calderwood, 2006) for all depths (see Supplementary Information Figure S2c) resulting in a somewhat lower correlation of 0.82.

In *Figure 2(d)*, we show profiles of the estimated effective creep viscosity for continents and oceans within the upper (300 km)~~mantle and the crust . The corresponding diffusion and dislocation creep estimates are shown in figure 2(d)~~ using olivine parameters modified after (Hirth and Kohlstedt, 2004) (Shown in the Appendix, Table A1. *Figure 2(d)* shows how a laterally averaged (dependent on depth only) asthenospheric viscosity decreases with increasing water content (i.e. 100, 500, 1000 H/10^6Si). The viscosities are averaged separately across the continental and oceanic regions *(Figure 2d*, dashed versus solid lines). The average oceanic viscosity profiles give lower values than the respective average continental viscosity (η_{eff}), within the depth range of 100 ± 60 km. Seismological studies (e.g. Schaeffer and Lebedev, 2013; Kawakatsu et al., 2009; Fischer et al., 2010; Rychert et al., 2005) show this as a seismic wave velocity drop (~$5-10\,\%$), and as a transition between the lithosphere and asthenosphere corresponding to the low viscosity channel *(Figure 2d)*. Figure 2(c) shows tractions causing stresses and topography in the lithosphere from the simulation using the creep parameters that correspond to the green effective viscosity profile in *Figure 2(d)*, which was used ~~for~~ to model the dynamic geoid and plate motions. Here, at all plate boundaries we have used a friction coefficient $\mu = 0.02$ within the crust and lithospheric layers to generate the global plate velocities in a No-Net-rotation (NNR) reference frame shown in Figure 2(b) with RMS of 3.5 cm/yr. Since the focus of this study is to investigate the effect of the upper mantle lateral density variations on the horizontal stress field and dynamic topography, an assessment of the influence of the plate boundary friction and water content in the asthenosphere on plate velocities has been carried out in a separate study (Osei Tutu et al., 2018). Hence, in the present work, we constrain our resulting creep viscosity with a cutoff for extreme viscosity values in the upper mantle by setting permissible minimum and maximum viscosity values similar to Becker (2006) and Osei Tutu et al. (2018), with this approach yielding a good fit between the observed and modeled geoid.

3.2 Shallow and deep contributions to the crustal stress state

We start with examining separate contributions of the mantle heterogeneities below 300 km (deep Earth setup) and above (shallow Earth setup) to the global lithospheric stress field and topography. To calculate the contribution of the lower domain, we use a constant lithosphere thickness (100 km) and density (3.27 kg/m^3), with similar configuration of the mantle

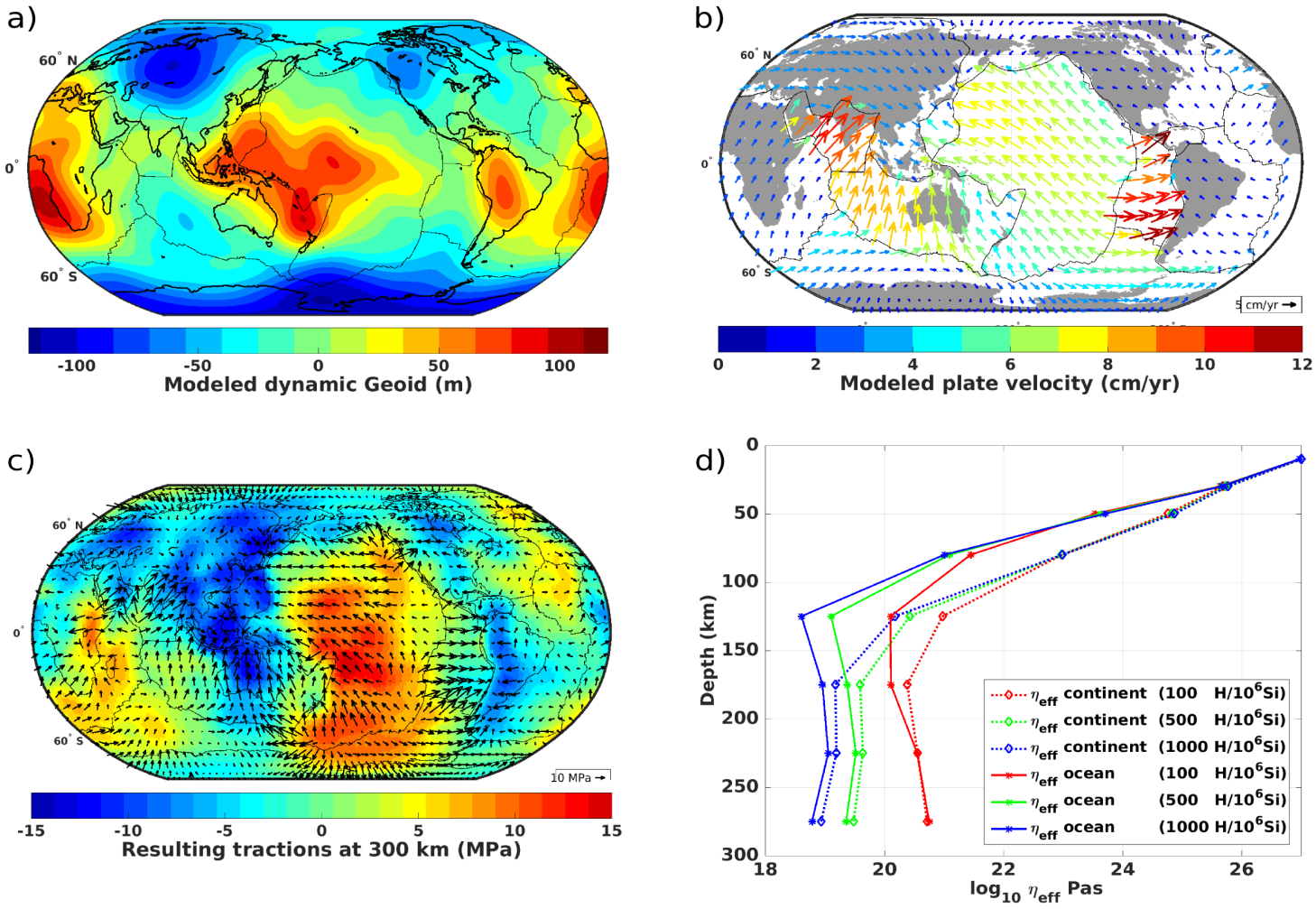

Figure 2. *(a) Modeled geoid anomaly and (b) modeled plate velocity, considering lateral viscosity variations with the TM1 thermal-density model in the upper 300 and a 3-D density structure of the mantle inferred from Becker and Boschi (2002) in combination with the layered viscosity profile from Steinberger and Calderwood (2006) imposed below 300 km. (c) Resulting total shear tractions at the 300 km depth generating stresses in the lithosphere. (d) The corresponding average creep viscosity versus depth in the upper mantle across continents and oceans, considering different olivine parameters.*

below as used to prescribe the geoid anomaly, plate motions and the shear tractions (Figure 2a-c). ~~a radial viscosity distribution shown in Figure 1(b) and a seismic velocity-to-density scaling (Figure 1a) below a depth of 300 km following Steinberger and Calderwood (2006) and a 3D density structure below depth 300 km derived from the seismic tomography model Smean (Becker and Boschi, 2002).~~ The resulting maximum horizontal magnitude (SH_{max}) and direction of the lithospheric stress field ~~and the resulting dynamic topography are~~ *is* shown in Figure 3a ~~and 3c~~. We have obtained compressional regimes in regions of past and present subduction. In the North and South American continents, beneath which the ancient Farallon and Nazca plates were subducted, compressive stress magnitudes reach about 40 MPa. In the Far East, downwelling flows stretching from north to south from the northwestern Pacific through Australia towards Antarctica create compressional stress regimes with magnitudes ranging between ~ 50 and 80 MPa. These compressional regions are connecting the Arctic with Antarctica and engulf two distinct regions with extensional stress regimes centered on the Pacific and African superswell regions. The predicted SH_{max} directions in Figure 3(a) generally follow the first-order lithospheric stress pattern (Zoback 1992), similar to previous mantle flow predictions of lithospheric stresses (Steinberger et al., 2001; Lithgow-Bertelloni and Guynn, 2004; Ghosh and Holt, 2012). In the largest extensional regions such as found in the Pacific superswell and above deep upwellings across southeastern Africa, stresses reach magnitudes of around 30 MPa. The modeled extensional/compressional pattern in the constant lithosphere, which get smoothed out over large distance are induced by the gradient in the tractions (Figure 2c) coming from the mantle flow.

To investigate the contribution of the upper domain (300 km) to the stress field, we calculate the magnitude and direction using model TM1 (Figure 1d) combined with the CRUST 1.0 model (Laske et al., 2013) and disregarding mantle density variations below 300 km (i.e. both horizontal and vertical tractions below the depth of 300 km are set to zero). Comparison of the lithosphere stress predictions from our shallow (Figure 3a) and deep (Figure 3b) Earth setups reveals notable differences in the model-based stress regimes, magnitudes and directions in continental regions. If stresses are generated by the upper domain only, then almost all continental regions are characterized by an extensional regime, with the largest stress magnitudes found in areas of high topography and orogenic belts, such as the Tibet and Andes highlands. Our stress predictions from the shallow Earth setup with laterally varying crustal and lithospheric densities in Figure 3(b) show stress magnitudes and patterns similar to Naliboff et al. (2012). However, as opposed to the results of Naliboff et al. (2012) we predict high compressional stress magnitudes at continental margins, which may in part originate from a finer treatment of the crust and our temperature-dependent creep viscosity. Also the high compressional stresses along the subduction margins in Figure 3(b) are likely induced by the slab models included in our setup. ~~Figure 3(d) shows~~ *The resulting topographies beneath air (free surface) accompanying either predicted lithospheric stress field is shown in Supplementary Information Figures S3(a-b).*

3.3 Total lithospheric stresses and topography

Next we compute the combined effect of both the lower mantle buoyancy and the upper mantle heterogeneities on the global SH_{max} magnitude and direction for comparison with the separate contributions discussed above and with observations. Note that this is not a linear superposition of the separate contributions, because changes in the properties of the upper 300 km lead to changes in the topography and stress caused by density anomalies below 300 km depth. The resulting SH_{max} direction and

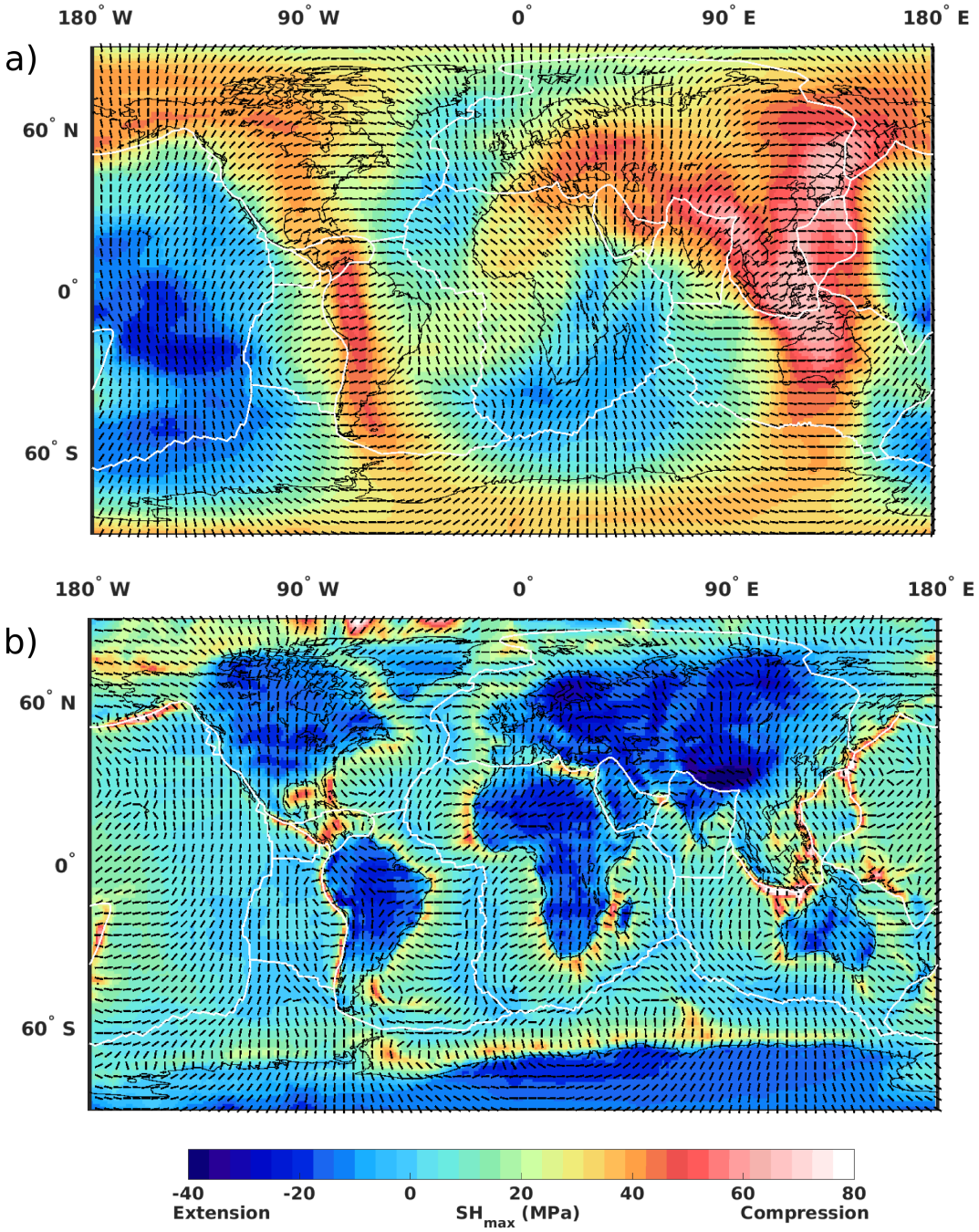

Figure 3. a) Model-based maximum horizontal stress magnitude and most compressive stress directions [SH_{max}] following the convention with compression being positive, originating from mantle flow driven by density anomalies below 300 km. (b) Same for structure of the top 300 km of the upper mantle, computed with the CRUST 1.0 model and TM1 ~~(c) and (d) depict the corresponding topography~~ beneath air (free surface).

magnitude (Figure 4a) due to the combined contributions of the upper and lower mantle show compressional regimes in areas similar to Figure 3(a), while muting almost all strong extensional stresses predicted by our simulation with the shallow Earth setup in continents (Figure 3b). Also, the predicted SH_{max} orientation generally follows the first-order lithospheric stress pattern (Zoback, 1992), similar to predictions based on only density anomalies below the 300-km depth (Figure 3a), with some regional deviations. The dominance of the contribution from below 300 km to the lithospheric stress field orientation becomes apparent when looking at the similarities between the SH_{max} directions in Figures 3(a) and 4(a) and dissimilarities with Figure 3(b), especially in continents. Nevertheless, the contribution from the upper 300 km to the predicted stress magnitude is evident in areas with large crustal thickness in continents, such as Tibet and the Andes. The regions where extensional regimes are predicted with only the contribution from below 300 km (Figure 3a) correspond well with the extensional stress regions in the combined model (Figure 4a).

The result is not very different, when we use the thermal density model TM2 for the total lithospheric stress field prediction. Both the predicted SH_{max} magnitude and direction with TM1 (Figure 4a) and TM2 (Figure 3b) show notable similarities in oceans and continents, owing to the strong contributions from below 300 km which are similar for both models. They show relatively high compressional stress magnitudes in subduction or convergence regions such as the Mediterranean, south of the Tibetan Plateau, south of Alaska, and the northwest Pacific extending through the Sumatra subduction zone and underneath the Australian and Antarctic plates. However, the SH_{max} compressional signal underneath North America in Figure 4(a) is muted and that of the South American region turns into an extensional regime along the Andes (Figure 4) with the inclusion of the mantle above 300 km and the crust. Similar to Figure 3(a) both predictions with TM1 and TM2 (Figures 4a and 4b) show SH_{max} extensional regimes corresponding to the regions of upwellings and/or volcanism. However, the model with TM2 generates a much higher extensional magnitude of ~60 MPa in the North Atlantic region around Iceland, and around the Azores and Canary hotspots, compared to TM1. Stress magnitudes are more alike in the Southern Pacific Rise and around southern Africa. Differences are in part due to the detailed and well resolved upper mantle structures in the S-wave model used to derive TM2 (Schaeffer and Lebedev, 2013), as opposed to the upper mantle structure in TM1, which is based on the sea floor age in oceanic regions (Müller et al., 2008) and slab temperatures from Steinberger (2000). Also in regions where the coverage of heat flow data is poor (e.g. in South America and Antarctica, (Artemieva, 2006; Pollack et al., 1993)), TM2 (Figure 3b) may give better results. TM2 predicts compressional stress under Antarctica and along the subducting Nazca plate in South America induced by downwelling flow. In these regions there are barely any heat flow data and TM1 remains largely unconstrained. Both modeling setups with the combined effects from the crustal structure model, the upper mantle thermal-density structure (either TM or TM2) and deep mantle contributions give topography *(Supplementary Information Figures S4a-b)* similar to actual topography. ~~Comparing the similarities between Figure 4(c-d) to Figure 3(d) shows much of the Earth's topography comes from density variations at shallow depths < 300 km.~~

3.4 Modeled versus observed lithospheric stress field

We compare our predicted SH_{max} orientation to the observational stress data. Following the stress interpolation method presented by Müller et al. (2003), we used their Fixed Search Radius (FSR) method which uses a global weighting defined by

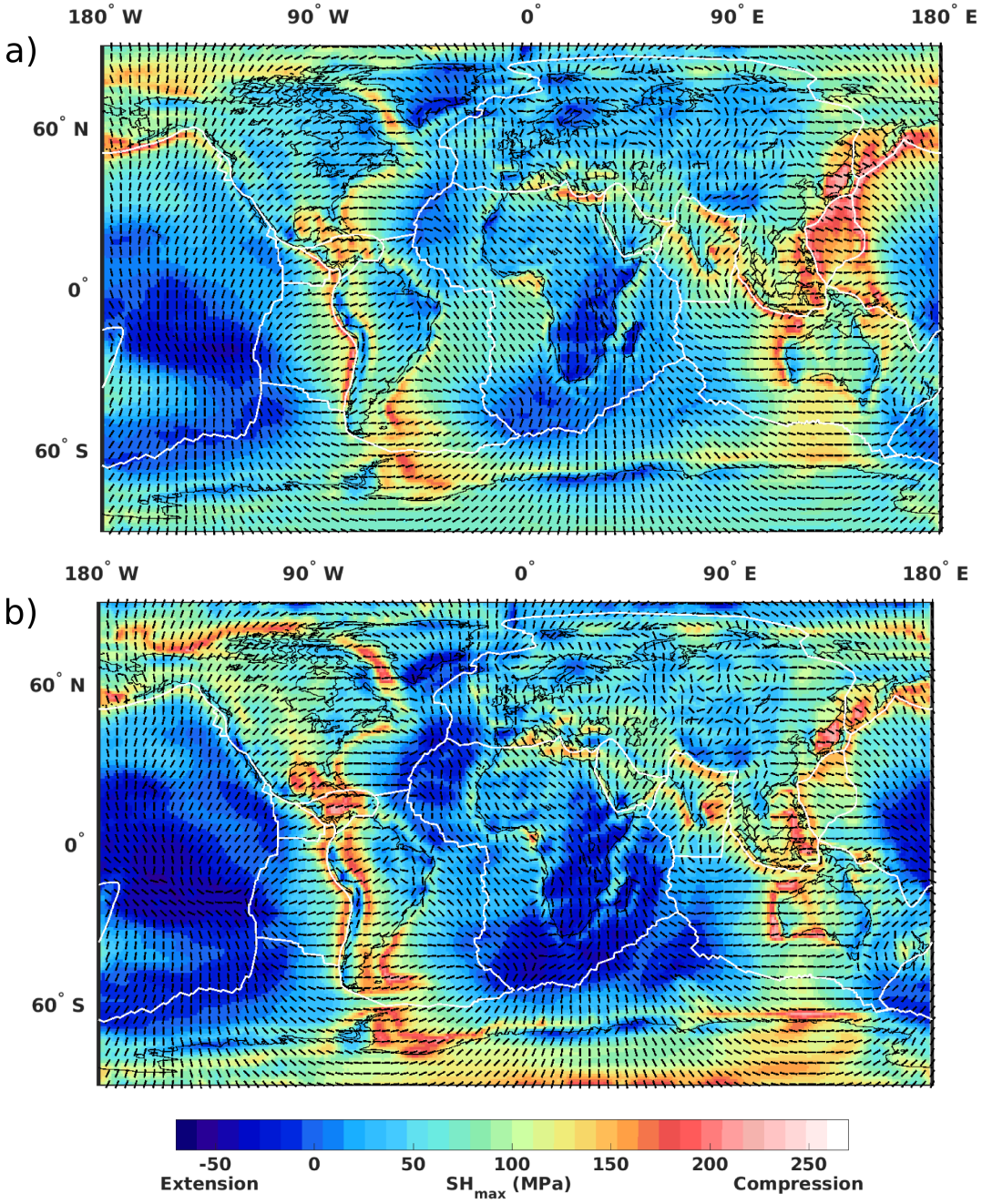

Figure 4. Predictions of the SH_{max} magnitude and direction from combined contributions due to lower mantle flow and upper mantle from a) TM1 with crust model and b) TM2 with crust model. ~~The corresponding model topographies are is shown in c) and d) respectively~~.

a fixed Euclidean distance for the stress data interpolation and stress quality. The smoothed stress field orientation at a grid point is based on the dominant stress data orientation within the selected radius. For a detailed explanation on the FSR method see Müller et al. (2003). Stress data with quality A, B, and C with known stress regime were considered. Since we do not consider the respective regime in our quantitative analysis, we also included the stress data with unknown style having quality A and B in our smoothing procedure to make our smooth field more robust. We smoothed the observed SH_{max} orientation of the World Stress Map 2016 (WSM2016) (Heidbach et al., 2016), with a search radius of 270 km *(Figure 5a)* on a grid interval of 2.5° x 2.5°. The background dot colors in the smoothed map represent the stress data regimes with red denoting normal fault, blue as thrust fault, green as strike-slip fault and black as unknown regime. For the interpolation we only took into account the orientation pattern of the stress data. We limit our comparison with modeled lithospheric stress orientation to areas with enough data for interpolation. The new WSM2016 has a relatively good coverage in some regions that were not well covered in the previous version (Heidbach et al., 2008) such as Brazil, parts of North America, Eastern Russia, and Central Africa. We regard it as appropriate to compare the modeled stress orientation with the smoothed observational stress data and regard deviations of actual stress from smoothed stresses as a second-order pattern.

3.4.1 Angular misfit between WSM2016 and modeled lithospheric stress

In Figure 5(b) we have superimposed our total modeled stress fields with the TM1 results depicted by thin bars and plotted on top of the TM2 results shown by thick bars, showing relatively good agreement of the stress pattern and regime at longer wavelength. However, the smaller-scale contribution from the upper 300 km generates regional variations in the stress pattern and regimes, which are mainly due to density contrasts in the lithosphere or underneath (which are nearly isostatically compensated or cause lithosphere flexure) and due to topography (Zoback, 1992; Zoback and Mooney, 2003; Bird et al., 2006). Compared to the observed SH_{max} patterns and regimes (Figure 5a) we predict similar styles in regions such as eastern Africa and Tibet with normal faulting comparable to earlier works that considered the effect of the whole mantle including lithosphere and crustal models (Lithgow-Bertelloni and Guynn, 2004; Ghosh and Holt, 2012; Ghosh et al., 2013; Wang et al., 2015). We predict normal faulting mostly in regions above upwellings (mostly extensional regions) such as the Icelandic swell, Eastern African rift, or along divergent plate boundaries, while thrust faults are mainly predicted in compressional regions such as subduction zones and some other tectonically active regions in continents.
To further evaluate the influence of each thermal structure we performed a quantitative comparison between modeled and smoothed observed stress orientations. The estimated angular misfit (Figure 6) is a measure of the minimum angle between the modeled lithospheric stress orientation (Figure 5b for TM1 and TM2) and smoothed observed stress orientation (Figure 5a), which ranges between 0° to 90°. Here, angular misfit lower than 22.5° is regarded as representing of a good agreement between the modeled and observed stress orientations, with values above 67.5° regarded as indicative of a poor fit. The general SSW to NNE stress orientation observed over the North American plate is matched by our model predictions with both thermal structures TM1 and TM2. The angular misfit maps over North America obtained with both thermal structures show a poor fit over the Yellowstone and Rocky Mountains extending to the Great Plains (Ghosh et al., 2013). The observed localized NW to SE stress direction deviates (Figure 5a) from the predicted long-wavelength stress pattern (Ghosh et al.,

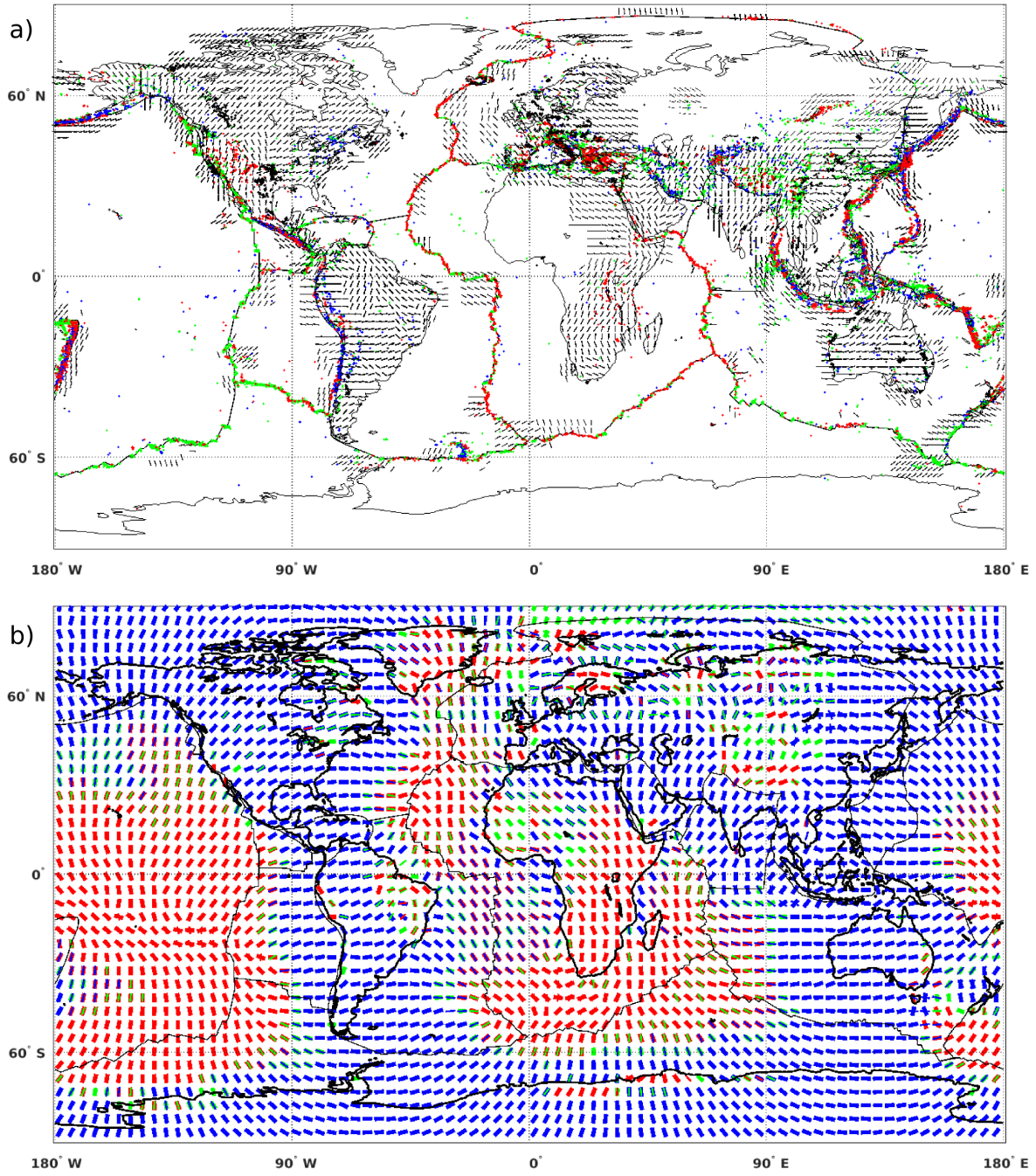

Figure 5. *(a) Interpolated World stress map 2016 (Heidbach et al., 2016), data on a grid of* $2.5^{\circ}x2.5^{\circ}$*, using only stress orientation with a constant search radius 270 km, and (b) predicted* SH_{max} *orientation and regime from total stress contribution with TM1 (plotted in thin bars) over TM2 (thick bars) upper mantle thermal structures. Colors of dots (a) and bars (b) indicate observed or predicted stress regime with red for normal faults or tensile stress, blue for thrust faults or compressive stress, and green for strike-slip faults or intermediate stress (one principal horizontal stress positive, one negative)*

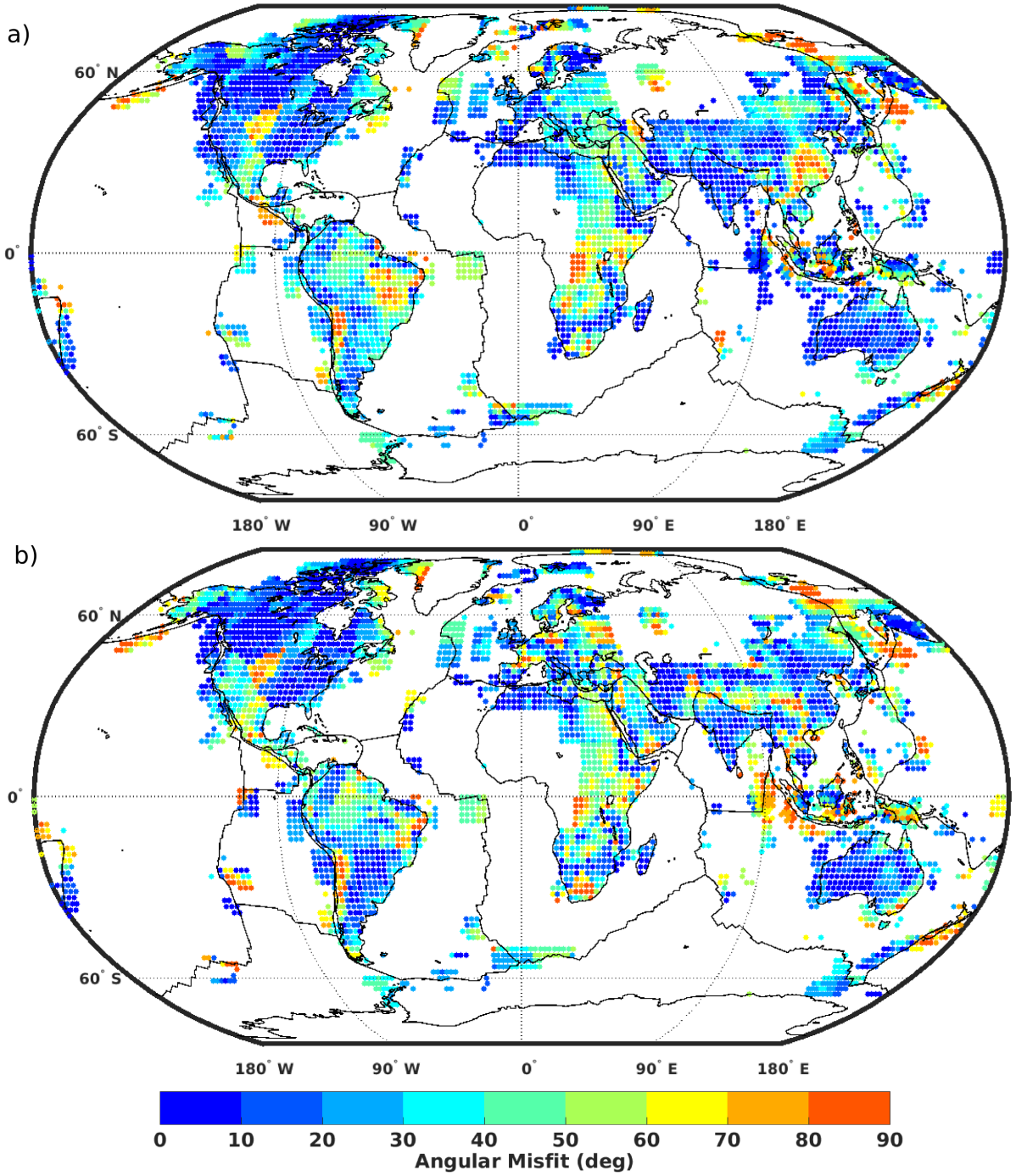

Figure 6. Angular misfit between the observed (WSM 2016) and total modeled stress directions with (a) TM1 and (b) TM2 upper mantle thermal and density structures.

2013; Humphreys and Coblentz, 2007). Even though the thermal model TM2 includes high-density cratonic roots, compared to TM1, their respective results for the angular misfits show that the North American cratonic root has a limited influence on the stress field. The two density structures TM1 and TM2 yield mean values of 22.2° (std = 19.6°) and 22.9° (std = 20.7°), respectively. As the upper mantle thermal structure TM1 for the South American continent is not well-constrained, due to lack of heat flow data, the predicted stress field in continental Brazil gives a relatively poor fit, with a mean misfit of 37.73° (std =20.24°). However, TM2 does not perform much better resulting in a mean misfit of 33.79° (std = 21.9°). Both models fail to match the observed stress field in the Andes, where a dominant localized N-S orientation is predicted, mainly as a results of the high topography and large crustal thickness (compare to Figure 8c-d). In the African continent, predicted N-S stress orientations along the Eastern African Rift from either model match the observed stress quite well with TM1 fitting observations much better compared to TM2 around the Ethiopian-Somalian-Yemen region, but both fail over the Congo craton and the South African plateau.

The stress field in western Europe is influenced by the North Atlantic ridge (NAR) push in the west and possibly by the far-field slab pull from the north-western Pacific subduction zones, while in the south, the driving forces are induced by the convergence of the African and Eurasian plates, with Africa subducting under Eurasia in the Mediterranean (Zoback, 1992; Müller et al., 1992; Gölke, 1996; Heidbach and Höhne, 2007; Schiffer and Nielsen, 2016). These plate boundary forces combined with the anomalous mantle pressure (Schiffer and Nielsen, 2016) underneath the North Atlantic lithosphere generate the dominant first-order NW-SE stress pattern. In our study, due to mantle contribution >300 km, we could match the NW-SE stress orientation nearly perfectly, with the model using TM1 (Figure 7a) showing small regional deviations, while the use of TM2 (Figure 7d) results in larger deviations from this NW-SE pattern in some regions.

These regional pattern deviations between modeled and observation orientations are mainly induced by differences in the upper mantle density structures and topography (Heidbach and Höhne, 2007) (compare to Figure 3a). The high density of heat flow data (Pollack et al., 1993; Artemieva, 2006) in continental Western Europe (TM1) improves the fit to the observed stress field compared to the thermal structure based on S-wave velocity (TM2) yielding mean misfit values of 18.30° (std = 22.67°) and 19.9° (std = 22.64°), respectively. Similarly, the large amount of heat flow data set in the Australian continent, improves the fit of the predicted intra-plate stress to the WSM2016 (Figure 7c, mean = 23.07° and std = 19.4°) compared to TM2 (Figure 7e, mean = 32.7° and std = 24.22°). It has been argued that the stress pattern in Australia is mainly driven by plate boundary forces (Reynolds et al., 2002), but based on the lithospheric and crustal structures used we show here that crustal and sub-lithospheric heterogeneities have a certain degree of influence. In the Tibetan region, the collision of India and Eurasia shows complex crustal and lithospheric deformation (van Hinsbergen et al., 2011; Gaina et al., 2015) generating NE-SW compressional stress. The SH_{max} predictions with TM1 (Figure 7c) fit better the stress pattern over the Tibetan Plateau with a mean value of 28° (std = 23°) compared to TM2, where a predicted E-W direction results in a misfit ~50° (Figure 7f). Both models performed relatively poorly over parts of China, when compared to the observed stress field.

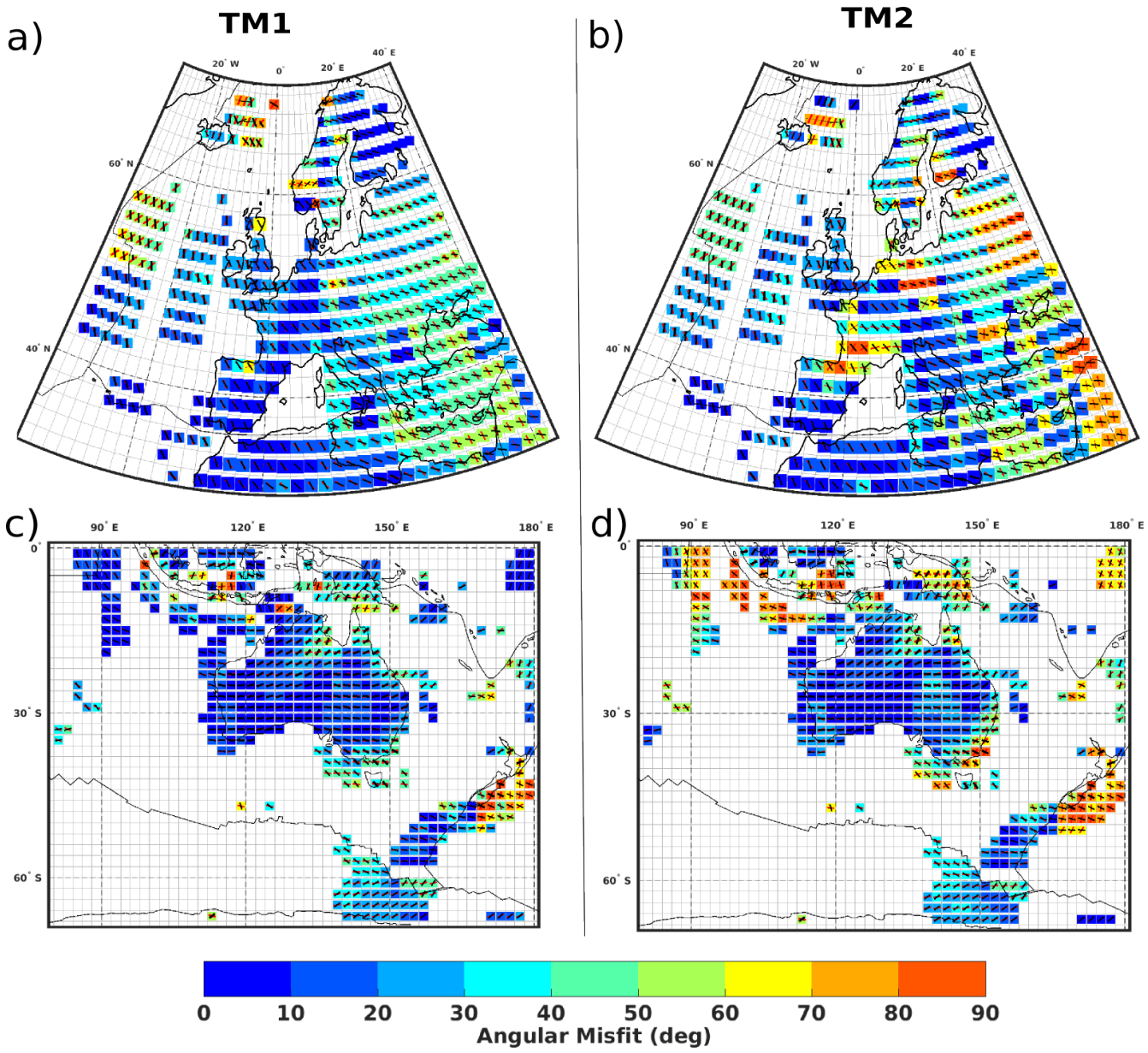

Figure 7. *Regional comparison of the angular misfit in Europe (a and b) and Australia (c and d) between the observed and modeled total stresses with TM1 (a-c) and TM2 (d-f). Red bars denote modeled orientations versus black bars showing the smoothed observed stress field (WSM2016).*

4 Modeled 'Dynamic' topography

Following the above prediction of lithospheric stress field ~~and topography~~, we repeated the two simulations to compute topography and SH_{max}, but this time without crustal thickness variations (Figure 8) to distinguish isostatic contributions form non-isostatic contributions.*The resulting stress magnitude and orientation from TM1 (Figure 8c) and TM2 (Figure 8d) without the crustal contribution are quite similar to the respective previous results that include the crustal contribution but giving some regional differences, for instance the N-S predicted stress orientation in the Andes in Figure 4(a-b) compared to Figure 8(c-d)*. Here, the resulting topographies with TM1 (Figure 8a) and TM2 (Figure 8b) show similar amplitudes due to the sea floor cooling and thickening along the ridges in the Atlantic, Indian and Pacific Oceans, peaking above ~1.5 km. With TM1, which explicitly contains subducted slabs, narrow, deep trenches are computed above subduction zones, such as in the northwestern Pacific and at the west coast of South America. Also the negative topography in the Sumatra plate boundary is reproduced well with the TM1 model reaching a value ~ -1.8 km. Based on tomography (model TM2) the computed topographic lows are wider and less prominent.

Predicted topography with TM2 is higher in eastern Africa (2 to 2.5 km), and highly elevated regions are more extensive. Figure 8(a) with TM1 (based on sea floor age) shows relatively low topography amplitudes in the northwest of the Pacific plate around Hawaii and towards the Mariana trench compared to Figure 8(b) with TM2 (based on the S-wave model SL2013sv) corresponding to a mean regional temperature difference of about ~200°C between TM1 and TM2 (Figure 1d-e). The 'dynamic' topography with TM2 replicates nearly all island chains associated with hotspots in and around the African plate, in the Pacific and along the Atlantic opening. In the North Atlantic, the positive topography (Icelandic swell) due to the Iceland plume-lithosphere interaction (Rogozhina et al., 2016; Schiffer and Nielsen, 2016) is more pronounced in Figure 8(b) with TM2 based on the tomography of Schaeffer and Lebedev (2013). Here the heights exceed 2 km as compared to Figure 8(a) with TM1 based on the ocean floor ages of Müller et al. (2008), showing values slightly below 2 km. The high isostatic topographic amplitudes along the mid-ocean ridges (MORs) as a result of high temperatures beneath these spreading centers where new sea floor is created are generally more pronounced in the TM2 model simulation than in the TM1 experiment. Despite the striking differences between topographic amplitudes in Figures 8(a) and 8(b) along the MORs, *the resulting* modeled stress orientations (Figure 8c-d) are very similar in these regions.

Also the large negative topography amplitude in cratons observed in dynamic topography with TM2 compared to TM1 does not readily translate into similarly large variations in the respective predicted SH_{max} orientation (Figure 8c-d), showing that cratonic roots have less influence on the lithospheric stress field (Naliboff et al., 2012). ~~Also, the predicted strong negative topography (Figure 8a-b) in continental regions such as North America, Eurasia, western Africa, South America, and western Australia are mostly due to mantle lithosphere in cratons.~~ *Low temperatures as shown in the thermal model TM2 (Figure 8b) translate to strong negative topographic anomalies, which are due to the conversion from seismic models to temperature and density, with the assumption that all seismic velocity anomalies are due to thermal variations only.* This produces unrealistically strong density anomalies and hence, large negative topography in cratons (Forte and Perry, 2000), if correction due to the chemical depletion in the mantle lithosphere is not considered. ~~Cammarano et al. (2011) showed that correction for~~

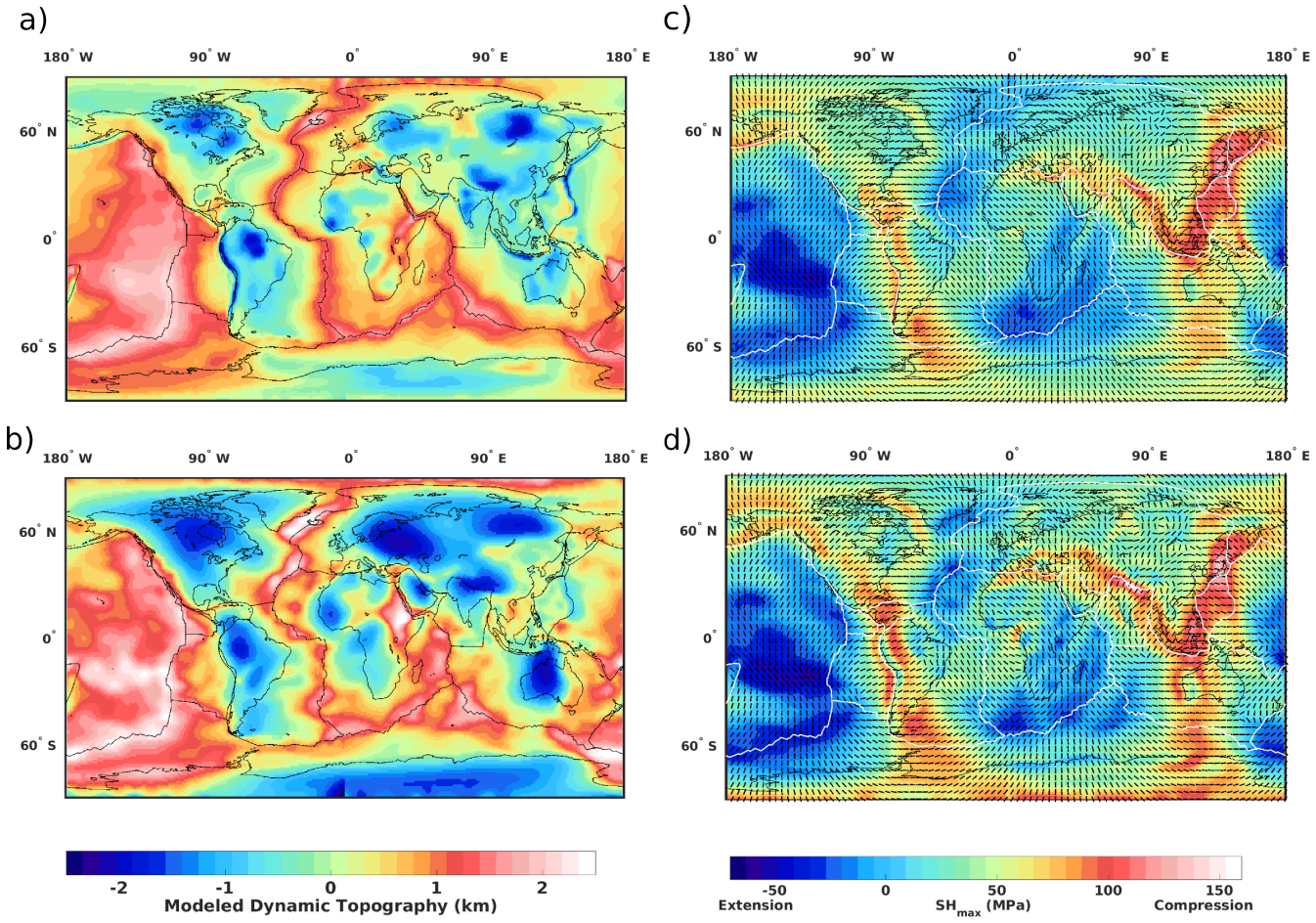

Figure 8. Modeled 'dynamic' topography using the upper mantle structure (a) TM1 and (b) TM2 and corresponding SH_{max} prediction with (c) TM1 and (d) TM2. In contrast to Figure 4, the effect of the crust is not included here.

~~the depletion of the lithosphere increases the inferred temperature of a cratonic root by about 100 K and decreases density by about 0.01 gcm^{-3}, and fits observations well compared to models assuming pyrolitic composition. Hence we adopt two additional thermal structures from different seismic tomography models SAW24B16 (Mégnin and Romanowicz, 2000) and S20RTS (Ritsema et al., 2011) with corrections applied to the depleted mantle based on Cammarano et al. (2011) and compare with our results.~~ *Previous studies of cratonic mantle depletion in-relation to density and temperature inferred from S-wave models for example, Cammarano et al. (2011) identified composition as the key dominant effect for the low modeled topography. They showed that with the assumption of only 100 K hotter mantle and laterally variations in composition resulted in a difference in density of about 0.1 gcm^{-3} compared to models assuming pyrolitic composition. The depletion-related density in cratons is age-dependent considered to be progressing from 30 to 80 kgm^{-3} (i.e. 0.03 to 0.08 gcm^{-3}) for Phanerozoic through Protozoic to Archean platforms. However, as a first order analysis an additional mean*

density value of 0.04 gcm^{-3} (about 300 K) as correction in TM2 cratons is considered to compare with models with realistic corrections. Also, following the realistic compositional correction in cratons by Cammarano et al. (2011) we adopt two additional thermal structures from different seismic tomography models SAW24B16 (Mégnin and Romanowicz, 2000) and S20RTS (?) with corrections applied to the depleted mantle based on and compare with our results. ~~A follow-up estimate of stresses and topography using TM2 with a constant temperature of 100 K applied as a correction to continental depletion in all major cratons is compared with observed fields.~~

4.1 Comparing the modeled dynamic topography to the observational-based residual topography.

Here, we compare our modeled dynamic topography to two independent observation-based residual topography fields (Hoggard et al., 2016; Steinberger, 2016). Residual topography gives a convenient way to constrain both isostatic and non-isostatic contributions to the modeled dynamic topography (Crough, 1978; Gurnis et al., 2000; Wheeler and White, 2000; Becker et al., 2014; Heidbach et al., 2016; Steinberger, 2016). This is done with the assumption that if topography is perfectly compensated isostatically within the upper mantle at depths within the range of 100 - 150 km, the integral of density with depth, as a function of crustal thickness and density to the Moho depth and of sea floor age will be the same everywhere for the chosen depth. The observation-based model by Hoggard et al. (2016) is derived from ocean seismic surveys (in-situ) in oceanic regions and free-air gravity anomaly data in continents (Figure 9a), while the residual topography model of Steinberger (2016) (Figure 9b) is derived with the CRUST 1.0 model (Laske et al., 2013). These two models are comparable in most oceanic regions, but give large mismatches in continents. For example, the subducting plate under South America induces a negative anomaly in Figure 9(b) but in the same region there is a positive anomaly in Figure 9(a) due to the free-air gravity data used across continents. Hence, we perform a regional quantitative comparison for oceans and continents separately. To compare the modeled dynamic topography from TM1 and TM2 simulations (Figure 8a and 8b) to the observed fields (Figures 9a and 9b), we first remove the height due to ocean floor cooling. This is done by subtracting the height estimates from sea floor age (Müller et al., 2008) from the modeled dynamic topography, using the relation $H_{topo} = 3300\text{m}\cdot(1 - \sqrt{\frac{age}{100Ma}})$. Here we assume a half-space cooling for the sea floor with age. For a smooth transition of topographic height from ocean to continent and to avoid large jumps we nominally assume a 200 Ma lithosphere age for continents following the approach of Steinberger (2016). The resulting modeled dynamic topography fields (Figure 9c-d) with the effect of the sea floor cooling with age removed, and with locations of active hotspot volcanism plotted as green dots show to which extent each of the models is able to predict the positive topographic amplitudes due to upwellings induced by plume heads pushing the lithospheric base.

A visual comparison of the two observation-based residual topography fields (Figure 9a-b) with the modeled topography (Figure 9c-d) shows some features that are well reproduced ~~with both the TM1 and TM2 models. Among them are~~ such as the Pacific Swell and the Hawaiian plume track, while the Canary Island plume, and the heights around south-eastern Africa are much better reproduced by the TM2-based dynamic topography (Figure 9d). Removing the height due to ocean floor age results in either zero or negative topographic amplitudes along MORs in the Atlantic and Indian Oceans in the TM1-based dynamic topography (Figure 9c), giving correlation of 0.323 and 0.198 (Table 1) in oceans to Steinberger (2016)(S2016) and

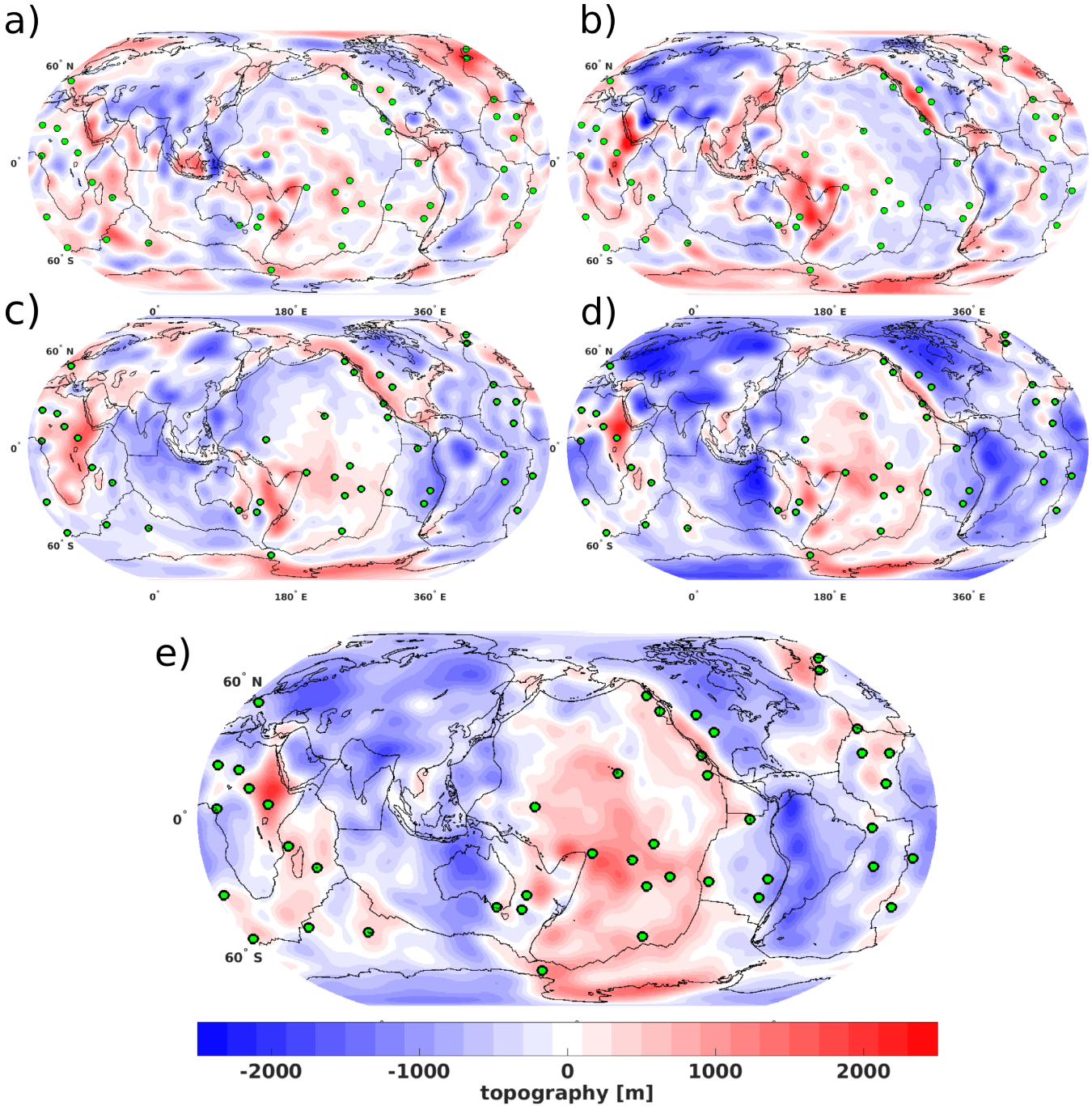

Figure 9. Comparing a) the in-situ observed residual topography from Hoggard et al. (2016), and b) the residual topography based on the CRUST 1.0 from Steinberger (2016) with modeled dynamic topography using TM1 (c) and TM2 (d) upper mantle thermal density structures with the effect of the sea floor cooling with age removed.(e) Similar modeled dynamic topography using TM2 upper mantle thermal density structures with constant temperature (100 K) added in cratons. Green dots with black circles around show locations of major hotspots. Green dots with black circles around show locations of major hotspots

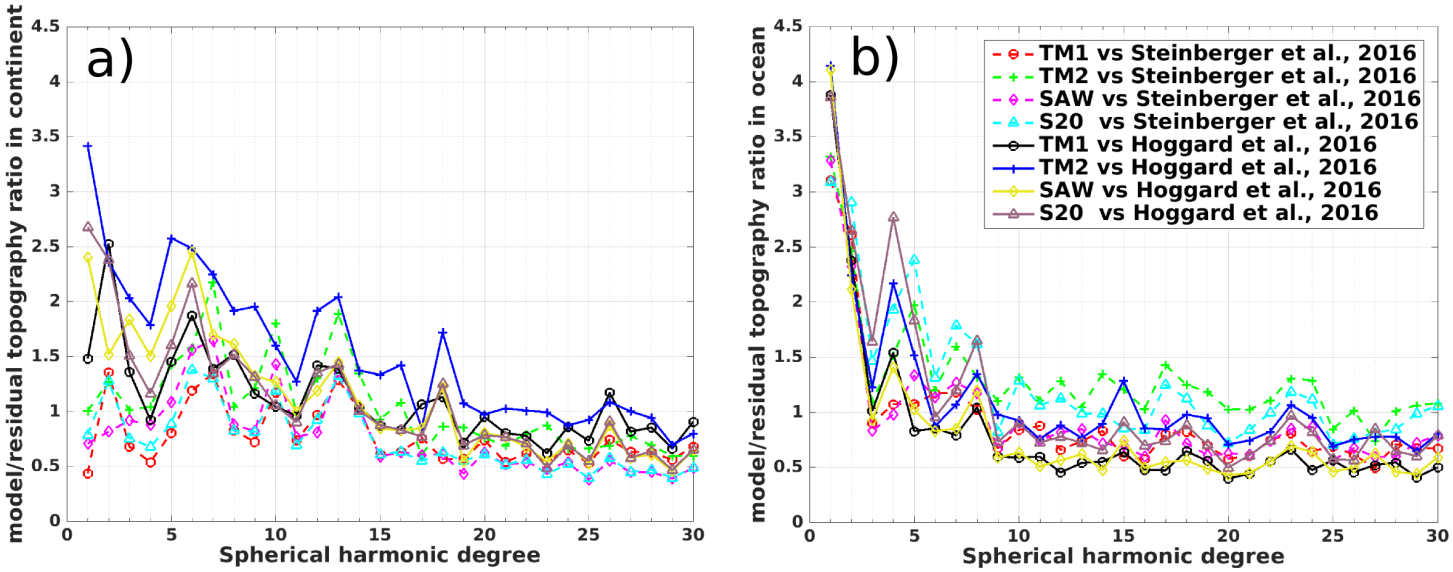

Figure 10. Ratio of modeled dynamic topography from TM1 and TM2 for (left) continental and (right) oceanic regions with observation-based residual topography from Steinberger (2016) and Hoggard et al. (2016)

Hoggard et al. (2016)(H2016), respectively. This model uses the thermal density structure derived from the ocean floor age in the upper 300 km; hence, when this contribution is removed, only the lower mantle contribution remains. In contrast, the TM2 model still gives small-scale topography anomalies (Figure 9d due to density anomalies other than from the sea floor cooling at depths above (300 km), which are resolved by the seismic model used to derive TM2 thereby giving relatively higher correlation to S2016 and H2016 of 0.348 and 0.284 in oceans respectively. To estimate the separate regional ratio between the modeled and observation-based residual topographies for continents and oceans, we assigned the mean continental amplitude in continental areas to estimate the degree by degree ratio for oceans only (Figure 10b) and vice-versa for oceanic regions to estimate continents ratio (Figure 10a).

In continents, the TM1 model (Figure 9c) is similar to the residual models (Figure 9b), exhibiting a correlation of 0.481 and a ratio of 0.98 (Figure 10a) up to the spherical harmonic degree 30. ~~red Over North America, Eurasia, and Australia it also fits the observed stress field better than TM2 (Figure 6)~~. The TM2 model gives similar ratio and correlation, but at degrees lower than 15 the TM2-induced modeled dynamic topography is about twice the amplitude of TM1 (Figure 10a). Over the African continent with far less heat flow data used to derive TM1, the thermal density structure gives a large continental uplift up to about 2 km, similar to parts of Antarctica (Figure 9c). In Figure 9(d) this uplift is less extended, better resolving the negative topography of the Congo craton but reaching a height above 2 km over the East African swell similar to S2016 (Figure 9b). Many of the remaining continental regions, however, show large negative topographic magnitudes of -2 km and more, resulting from neglecting the compositional effects in cratons (e.g. Eurasia, Australia and North America). The wide range of variations shown in degree 1 to 2 ratio for continents (Figure 10a) are due to the strong contributions coming from the

Table 1. Correlation the between modeled dynamic topography and the observation-based residual topography models (Steinberger, 2016; Hoggard et al., 2016) for continents and oceans.

modeled topography	Steinberger, 2016		Hoggard, 2016	
Upper mantle Thermal density	*Ocean*	*Continent*	*Ocean*	*Continent*
$1.TM1$	0.323	0.481	0.198	0.169
$2.TM2$	0.348	0.498	0.284	0.171
$3.TM2 + 100K\,(in cratons)$	0.370	0.512	0.284	0.180
$4.S20RTS(S20)$	0.442	0.653	0.221	0.232
$5.SAW24B16(SAW)$	0.248	0.718	0.287	0.188

different cratonic structures in each thermal model. *To further evaluate the impact of accounting for the correction due to chemical depletion in cratonic regions on the stress field and the dynamic topography, we have assumed additional 100 K converted to a negative density as compositional contribution in all cratons to the depth of 100 km of TM2 as opposed to the more realistic treatment of compositional effects as done for SAW and S20, with the method from Cammarano et al. (2011).*

The modeled topography shows improvements in cratonic regions (Figure 9e) but there is almost no change in the resulting lithospheric stress field (also see Supplementary figure S3). The correlation to S2016 increases to 0.512 for TM2 (with an assumed 100 K compositional effect) in continents. SAW and S20 give much higher correlation 0.653 and 0.718 in continents (Table 1), which could be a result of a more realistic treatment of cratonic regions but also of using different seismic tomography models. For example, Steinberger (2016) used a similar simple procedure to convert seismic velocities from different tomography models to density and still obtained a rather high correlation of 0.64 in continents.

The assumed compositional correction is not very large giving about a 100 m reduction in the cratonic negative anomaly (Figure 9e) compared to the case without correction in continents (Figure 9d). This in part supports the proposed treatment of the upper mantle thermal density structure with joint petrological and seismological constraints (Forte and Perry, 2000; Forte et al., 2010; Cammarano et al., 2011), which is outside the scope of our studies. The residual topography of Hoggard et al. (2016) shows positive amplitudes over the Eurasian craton due to the free-air gravity data used, while the other residual (Figure 9b) and all modeled dynamic topography models give negative values, resulting in a low correlation with H2016 on continents for all models. ~~Here the correlation with H2016 in oceanic regions is also lower except for SAW24B16. This result is model-dependent, and Steinberger et al. (2017) also find an improved correlation with H2016 in oceans using a different density model.~~

This is an improvement compared to much simpler representations of the upper mantle structure in previous studies using a thin-sheet/shell approximation (Steinberger et al., 2001; Lithgow-Bertelloni and Guynn, 2004; Ghosh and Holt, 2012; Ghosh

et al., 2013; Wang et al., 2015). Stresses induced by regional and global variations in the crustal and lithospheric structures are of the order of 100 MPa in magnitude across strongly uplifted continental areas (Artyushkov, 1973).

5 Conclusions

The aim of our study is to identify and quantify the influence of density anomalies and rheology in the crust and mantle on the present-day lithospheric stress field and dynamic topography. The focus is on anomalies and rheology above 300 km depth; therefore we use a number of different density structures, and nonlinear temperature and stress dependent rheology above 300 km: Our *first upper mantle thermal-density model (TM1)* is based on heat flow data on continents (Artemieva, 2006) and sea floor age (Müller et al., 2008) in the oceans, while *the second upper mantle thermal-density model TM2,* and several alternative models considered, are based on seismic tomography (Schaeffer and Lebedev, 2013; Ritsema et al., 2011; Mégnin and Romanowicz, 2000). In contrast, only one density structure, based on the SMEAN (Becker and Boschi, 2002) tomography, and a radial viscosity structure (Steinberger and Calderwood, 2006) is used below 300 km depth. A key feature that distinguishes our work from previous studies is the use of a coupled code (Sobolev, 2009) that considers density heterogenety in the entire mantle, along with a realistic lithosphere with free surface, such that lithosphere stresses are computed with a fully three-dimensional, rather than a thin-sheet approach.

Resulting lithosphere stresses are rather similar, both among the different models we consider, and to previously published results. They are also similar to a case where only the contribution from the mantle below 300 km is considered, showing that a larger portion of the contribution to the lithospheric stress field originates from mantle flow driven by density anomalies below 300 km depth (Steinberger et al., 2001; Lithgow-Bertelloni and Guynn, 2004). Only in some regions, particularly those with large and variable crustal thickness, such as Tibet, or the Altiplano, shallow contributions are dominant. The lower mantle stress contribution is dominated by very-large-scale structures, with stress directions remaining similar over thousands of kilometers. It is related to very-large scale mantle structures, which are well imaged by seismic tomography, causing overall similarity between our models and published ones.

We compare computed directions of maximum compressive stress with the World Stress Map, and find a rather good overall agreement, confirming previous comparisons. However, regional comparison highlights those areas where the fit remains poor: These include the Colorado Plateau, the Altiplano, parts of Brazil, the Congo Craton, and parts of China, thus highlighting regions on which future studies could focus. Computed stresses based on heat flow (Model TM1) compare more favorably to observations in those regions where heat flow coverage is good (e.g. Western Europe), whereas the stresses computed from tomography (Model TM2) give a better fit for regions of poor heat flow coverage, such as South America.

In contrast to stress field, density anomalies above 300 km depth contribute dominantly to dynamic topography. Therefore, dynamic topography is more variable among the different models we consider and differs more strongly from published models. Dynamic topography also has a larger contribution at smaller scales. Some of these contributions can be related to subducted slabs or mantle plumes. Confirming previous results, we find that negative topography in cratons is too large, unless a correction for the depletion of cratonic lithosphere is considered. The best fit can be obtained, if the method of Cammarano et al. (2011)

is used to convert seismic tomography models to temperature structures, taking chemical depletion in cratonic areas into account. The best agreement is found with residual topography on continents that considers crustal thickness variations based on CRUST1.0 (Laske et al., 2013) rather than deriving it from the gravity field. In order to fit either observable – stress or topography – attention has to be mostly paid to a detailed treatment of the Earth's parts – deeper or shallower – that give the largest contribution.

Appendix A: Rheology of the upper mantle and lithosphere

The coupling between the lithosphere and the mantle in our model allows for an implementation of realistic rheological parameters in both model domains. In SLIM3D, the stress- and temperature-dependent rheology is implemented according to an additive strain rate decomposition into the viscous, elastic and plastic components:

$$\dot{\varepsilon}_{ij} = \dot{\varepsilon}_{ij}^{vis} + \dot{\varepsilon}_{ij}^{el} + \dot{\varepsilon}_{ij}^{pl} = \frac{1}{2\eta_{eff}}\tau_{ij} + \frac{1}{2G}\hat{\tau}_{ij} + \dot{\gamma}\frac{\partial Q}{\partial \tau_{ij}} \tag{A1}$$

where G denotes the elastic shear modulus, $Q = \tau_{II}$ is the plastic potential function, $\hat{\tau}_{ij}$ is the objective stress rate, $\dot{\gamma}$ denotes the plastic multiplier, $\tau_{ij} = \sigma_{ij} + P\delta_{ij}$ is the Cauchy stress deviator, $P = -\sigma_{ii}/3$ is the pressure, $\tau_{II} = (\tau_{ij}\tau_{ij})^{1/2}$ stands for the effective deviatoric stress, and η_{eff} is effective creep viscosity derived by combining the diffusion and dislocation creep mechanisms, as follows:

$$\eta_{eff} = \frac{1}{2}\tau_{II}\left(\dot{\varepsilon}_{diff} + \dot{\varepsilon}_{disl}\right)^{-1} \tag{A2}$$

The effective scalar creep strain rates are given by Kameyama et al. (1999):

$$\dot{\varepsilon}_{diff} = \mathrm{A}_{diff} d^{-p} \left(C_{H_2O}\right)^{r_{diff}} \tau_{II} \left(\frac{E_{diff} + PV_{diff}}{RT}\right) \tag{A3}$$

$$\dot{\varepsilon}_{disl} = \mathrm{A}_{disl} \left(C_{H_2O}\right)^{r_{disl}} \left(\tau_{II}\right)^{n} \left(\frac{E_{disl} + PV_{disl}}{RT}\right) \tag{A4}$$

where the symbols A, E and V denote the experimentally prescribed pre-exponential factor, the activation energy and the activation volume, respectively, R denotes the gas constant, T is the temperature, n is the power law exponent, d is the grain size, and p is the grain size exponent, C_{H_20} is water content in ppm H/Si, and r_{diff} and r_{disl} are the water content exponents.

Along plate boundaries we account for the brittle deformation, with the yield stress defined according to the Drucker-Prager criterion based on the dynamic pressure:

$$\tau_{yield} = c + \mu P \tag{A5}$$

where c is the cohesion, μ is the coefficient of friction. Following Sobolev (2009) and

Table A1. The upper mantle creep viscosity is calculated using olivine parameters from the axial compression experiments of Hirth and Kohlstedt (2004). Crustal rheology is taken from (Wilks, 1990). The rheological parameters used in this study with varying Olivine water content of 100, 500, 1000 p.p.m H/10^6Si in the weak asthenospheric mantle with dry lithosphere material. For more details regarding the formulation of the physical model and numerical implementation the reader is referred to Popov and Sobolev (2008)

Parameter	Unit	Crust	Lithosphere (strong mantle)	Asthenosphere (weak mantle)
Bulk modulus K	GPa	6.3	12.2	12.2
Shear modulus G	GPa	4.0	7.40	7.40
Density ρ	gcm^{-3}	2.85	3.27	3.30
Cohesion c	MPa	5.0	5.0	5.0
Friction coefficient μ	-	0.6*	0.6*	0.6*
Diffusion creep parameters (d = 10 mm p = 3 r_{diff} = 1)				
A_{diff}	Pa^{-1}s^{-1}	-	$10^{-8.65}$	$10^{-8.82}$
Activation Energy E_{diff}	KJ/mol	-	375	335
Activation Volume V_{diff}	cm^{-3}/mol	-	6.0	4.0
Dislocation creep parameters Dislocation (r_{disl} = 1.2)				
A_{diff}	Pa^{-n}s^{-1}	$10^{-21.05}$	$10^{-15.19}$	$10^{-14.67}$
Activation Energy E_{diff}	KJ/mol	445	530	480
Activation Volume V_{diff}	cm^{-3}/mol	10.0	17.0	14.0
Power law exponent n	-	4.2	3.5	3.5

Code availability. The coupled global numerical code used to generate the results in this study builds on an in-house SLIM3D code (Popov and Sobolev, 2008) and spectral code (Hager and O'Connell, 1981) and is available upon request from any of the authors

Competing interests. The authors declare that they have no conflict of interest.

Acknowledgements. This work was supported by GeoSim grants under the Geo.X program in conjunction with GFZ-Potsdam, University of Potsdam and Free University of Berlin. Lastly, we thank the one anonymous reviewer and the Editor Taras Gerya for the constructive comments to improve our manuscript.

References

Artemieva, I.: Global $1^\circ \times 1^\circ$ thermal model $TC1$ for the continental lithosphere: implications for lithosphere secular evolution, Tectonophys., 416, 245–277, 2006.

Artyushkov, E. V.: Stresses in the lithosphere caused by crustal thickness inhomogeneities, J. Geophys. Res., 78, 7675–7708, 1973.

Becker, T. W.: On the effect of temperature and strain-rate dependent viscosity on global mantle flow, net rotation, and plate-driving forces, Geophys. J. Int., 167, 943–957, 2006.

Becker, T. W. and Boschi, L.: A comparison of tomographic and geodynamic mantle models, Geochem., Geophys., Geosys., 3, https://doi.org/10.1029/2001GC000168, 2002.

Becker, T. W., Faccenna, C., Humphreys, E. D., Lowry, A. R., and Miller, M. S.: Static and dynamic support of western (United State) topography, Earth Planet. Sci. Lett., 402, 234–246, 2014.

Bird, P. and Li, Y.: Interpolation of principal stress directions by nonparametric statistics: global maps with confidence limits, J. Geophys. Res., 101, 5435–5443, 1996.

Bird, P., Ben-Avraham, Z., Schubert, G., Andreoli, M., and Viola, G.: Patterns of stress and strain rate in southern Africa, J. Geophys. Res., 111, B08402, https://doi.org/10.1029/2005JB003882, 2006.

Bird, P., Liu, Z., and Rucker, W. K.: Stresses that drive the plates from below: Definitions, computational path, model optimization, and error analysis, J. Geophys. Res., 113, B11406, https://doi.org/10.1029/2007JB005460, 2008.

Brune, S., Popov, A. A., and Sobolev, S. V.: Modeling suggests that oblique extension facilitates rifting and continental break-up, Journal of Geophysical Research: Solid Earth, 117, B08402, https://doi.org/10.1029/2011JB008860, 2012.

Brune, S., Heine, C., Pérez-Gussinyé, M., and Sobolev, S. V.: Rift migration explains continental margin asymmetry and crustal hyperextension, Nature Communications, 5, 4014, https://doi.org/10.1038/ncomms5014, 2014.

Brune, S., Williams, S. E., Butterworth, N., and Müller, R. D.: Abrupt plate accelerations shape rifted continental margins, Nature, 5, 201–204, https://doi.org/10.1038/nature18319, 2016.

Burov, E. B.: Rheology and strength of the lithosphere, Marine and Petroleum Geology, 28, 1402–1443, 2011.

Čadek, O. and Fleitout, L.: Effect of lateral viscosity variations in the top 300 km of the mantle on the geoid and dynamic topography, Geophys. J. Int., 152, 566–580, 2003.

Cammarano, F., Tackley, P., and Boschi, L.: Seismic, petrological and geodynamical constraints on thermal and compositional structure of the upper mantle: global thermo-chemical models, Geophys. J. Int., 187, 1301–1318, 2011.

Conrad, C. P. and Lithgow-Bertelloni, C.: Influence of continental roots and asthenosphere on plate-mantle coupling, Geophys. Res. Lett., 33, https://doi.org/10.1029/2005GL02562, 2006.

Crough, S. T.: Thermal origin of mid-plate hot-spot swells, Geophysical Journal of the Royal Astronomical Society, 55, 451–469, https://doi.org/10.1111/j.1365-246X.1978.tb04282.x, 1978.

Dannberg, J. and Sobolev, S. V.: Low-buoyancy thermochemical plumes resolve controversy of classical mantle plume concept, Nature Communications, 6, 6960, https://doi.org/10.1038/ncomms7960, 2015.

Davies, G. F.: Viscous mantle flow under moving lithospheric plates and under subduction zones, Geophysical Journal International, 49, 557, https://doi.org/10.1111/j.1365-246X.1977.tb01303.x, 1977.

Ebinger, C. J. and Sleep, N. H.: Cenozoic magmatism throughout east Africa resulting from impact of a single plume, Nature, 395, 788–791, 1998.

Faccenna, C., Heuret, A., Funiciello, F., Lallemand, S., and Becker, T. W.: Predicting trench and plate motion from the dynamics of a strong slab, Earth Planet. Sci. Lett., 257, 29–36, 2007.

Fischer, K. M., Ford, H. A. Abt, D. L., and Rychert, C. A.: The Lithosphere-Asthenosphere Boundary, Ann. Rev. Earth Planet. Sci., 38, 551–575, 2010.

Flament, N., Gurnis, M., and Müller, R. D.: A review of observations and models of dynamic topography, Lithosphere, 38, 189–210, https://doi.org/10.1130/L245.1, 2012.

Forte, A. M. and Mitrovica, J. X.: Deep-mantle high-viscosity flow and thermochemical structure inferred from seismic and geodynamic data, Nature, 410, 1049–1056, 2001.

Forte, A. M. and Perry, H. K. C.: Geodynamic Evidence for a Chemically Depleted Continental Tectosphere, Science, 290, 1940–1944, 2000.

Forte, A. M., Quere, S., Moucha, R., Simmons, N. A., P., S., Grand, S. P. Mitrovica, J. X., and Rowley, D. B.: Joint seismic-geodynamic-mineral physical modelling of African geodynamics: A reconciliation of deep-mantle convection with surface geophysical constraints, Earth Planet Sci. Lett., 295, 329–341, 2010.

Gaina, C., van Hinsbergen, D. J. J., and Spakman, W.: Tectonic interactions between India and Arabia since the Jurassic reconstructed from marine geophysics, ophiolite geology, and seismic tomography, Tectonics, 34, 875–906, https://doi.org/10.1002/2014TC003780, 2015.

Garcia-Castellanos, D. and Cloetingh, S.: Modeling the Interaction between Lithospheric and Surface Processes in Foreland Basins (in Tectonics of Sedimentary Basins: Recent Advances), pp. 152–181, John Wiley and Sons, Ltd, Chichester, UK, https://doi.org/10.1002/9781444347166.ch8, 2011.

Ghosh, A. and Holt, W. E.: Plate motions and stresses from global dynamic models, Science, 335, 839–843, 2012.

Ghosh, A., Holt, W. E., Wen, L., Flesch, L. M., and Haines, A. J.: Joint modeling of lithosphere and mantle dynamics elucidating lithosphere-mantle coupling, Geophys. Res. Lett., 35, L16309, https://doi.org/10.1029/2008GL034365, 2008.

Ghosh, A., Becker, T. W., and Humphreys, E. D.: Dynamics of the North American continent, Geophys. J. Int., 194, 651–669, 2013.

Gölke, M. C. D.: Origins of the European regional stress field, Tectonophysics, 266, 11–24, https://doi.org/10.1029/2011GC003934, 1996.

Gurnis, M., Mitrovica, J. X., Ritsema, J., and van Heijst, H.-J.: Constraining mantle density structure using geological evidence of surface uplift rates: The case of the African Superplume, Geochemistry, Geophysics, Geosystems, 1, https://doi.org/10.1029/1999GC000035, 2000.

Hager, B. H. and O'Connell, R. J.: A simple global model of plate dynamics and mantle convection, J. Geophys. Res., 86, 4843–4867, 1981.

Hager, B. H., Clayton, R. W., Richards, M. A., Comer, R. P., and Dziewoński, A. M.: Lower mantle heterogeneity, dynamic topography and the geoid, Nature, 313, 541–545, 1985.

Heidbach, O. and Höhne, J.: CASMI-A visualization tool for the World Stress Map database, Computers and Geosciences, 34, 783–791, 2007.

Heidbach, O., Tingay, M., Barth, A., Reinecker, J., Kurfeß, D., and Müller, B.: The World Stress Map database release 2008, https://doi.org/10.1594/GFZ.WSM.Rel2008, 2008.

Heidbach, O., Rajabi, M., Ziegler, M., Reiter, K., and Team, W.: The World Stress Map Database Release 2016 -Global Crustal Stress Pattern vs. Absolute Plate Motion, Geophys. Res. Abs., 18, EGU2016–4861,2016, 2016.

Heine, C., Müller, R. D., Steinberger, B., and Torsvik, T. H.: Subsidence in intracontinental basins due to dynamic topography, Physics of the Earth and Planetary Interiors, 171, 252–264, 2008.

Hirth, G. and Kohlstedt, D. L.: Rheology of the Upper Mantle and the Mantle Wedge: A View From the Experimentalists, in: Inside the Subduction Factory, edited by Eiler, J., vol. 138 of *Geophys. Monograph*, pp. 83–105, American Geophysical Union, Washington DC, 2004.

Hoggard, M. J., White, N., and Al-Attar, D.: Global dynamic topography observations reveal limited influence of large-scale mantle flow, Nature Geoscience, 9, 456–463, https://doi.org/10.1038/ngeo2709, 2016.

Humphreys, E. D. and Coblentz, D. D.: North American dynamics and western U.S. tectonics, Reviews of Geophysics, 45, 2005RG000 181, https://doi.org/10.1029/2005RG000181, 2007.

Kameyama, M., Yuen, D. A., and Karato, S.: Thermal-mechanical effects of low-temperature plasticity (the Peierls mechanism) on the deformation of a viscoelastic shear zone, Earth Planet. Sci. Lett., pp. 159–172, 1999.

Kawakatsu, H., Kumar, P., Takei, Y., Shinohara, M., Kanazawa, T., Araki, E., and Suyehiro, K.: Seismic Evidence for Sharp Lithosphere-Asthenosphere Boundaries of Oceanic Plates, Science, 324, 499–502, 2009.

King, S. D. and Ritsema, J.: African Hot Spot Volcanism: Small-Scale Convection in the Upper Mantle Beneath Cratons, Science, 209, 1137–1140, https://doi.org/10.1126/science.290.5494.1137, 2000.

Kreemer, C., Holt, W. E., and Haines, A. J.: An integrated global model of present-day plate motions and plate boundary deformation, Geophys. J. Int., 154, 5–34, 2003.

Laske, G., Masters., G., Ma, Z., and Pasyanos, M.: Update on CRUST 1.0 - A 1-degree Global Model of Earth's Crust, Geophys. Res. Abstr., 15, abstract EGU2013-2658, 2013.

Lithgow-Bertelloni, C. and Guynn, J. H.: Origin of the lithospheric stress field, J. Geophys. Res., 109, https://doi.org/10.1029/2003JB002467, 2004.

Lithgow-Bertelloni, C. and Silver, P. G.: Dynamic topography, plate driving forces and the African superswell, Nature, 395, 269–272, https://doi.org/10.1038/26212, 1998.

Marquart, G. and Schmeling, H.: Topography and Geoid Undulations Caused By Small-Scale Convection Beneath Continental Lithosphere of Variable Elastic Thickness, Geophysical Journal International, 97, 511–527, https://doi.org/10.1111/j.1365-246X.1989.tb00520.x, 1989.

Mégnin, C. and Romanowicz, B.: The three-dimensional shear velocity structure of the mantle from the inversion of body, surface, and higher-mode waveforms, Geophys. J. Int., 143, 709–728, 2000.

Müller, B., Zoback, M. L., Fuchs, K., Mastin, L., Gregersen, S., Pavoni, N., Stephansson, O., and Ljunggren, C.: Regional patterns of tectonic stress in Europe, Journal of Geophysical Research: Solid Earth, 97, 11 783–11 803, https://doi.org/10.1029/91JB01096, 1992.

Müller, B., Wehrle, V., Hettel, S., Sperner, B., and Fuchs, K.: A new method for smoothing orientated data and its application to stress data, Geological Society, London, Special Publications, 209, 107–126, https://doi.org/10.1144/GSL.SP.2003.209.01.11, 2003.

Müller, R. D., Sdrolias, M., Gaina, C., and Roest, W. R.: Age, spreading rates and spreading asymmetry of the world's ocean crust, Geochem., Geophys., Geosys., 9, Q04006, https://doi.org/10.1029/2007GC001743, 2008.

Naliboff, J., Lithgow-Bertelloni, C., Ruff, L., and de Koker, N.: The effects of lithospheric thickness and density structure on Earth's stress field, Geophysical Journal International, 188, 1–17, https://doi.org/10.1111/j.1365-246X.2011.05248.x, 2012.

Osei Tutu, A., Sobolev, S. V., Steinberger, B., Popov, A. A., and Rogozhina, I.: Evaluating the Influence of Plate Boundary Friction and Mantle Viscosity on Plate Velocities, Geochemistry, Geophysics, Geosystems, https://doi.org/10.1002/2017GC007112, http://dx.doi.org/10.1002/2017GC007112, 2018.

Pekeris, C. L.: THERMAL CONVECTION IN THE INTERIOR OF THE EARTH, Geophysical Journal International, 3, 343–367, https://doi.org/10.1111/j.1365-246X.1935.tb01742.x, 1935.

Pollack, H. N., Hurter, S. J., and Johnson, J. R.: Heat flow from the Earth's interior: Analysis of the global data set, Reviews of Geophysics, 31, 267–280, https://doi.org/10.1029/93RG01249, 1993.

Popov, A. and Sobolev, S. V.: SLIM3D: A tool for three-dimensional thermomechanical modeling of lithospheric deformation with elasto-visco-plastic rheology, Phys. Earth Planet. Inter., 171, 55–75, https://doi.org/10.1016/j.pepi.2008.03.007, 2008.

Popov, A. A., Sobolev, S. V., and Zoback, M. D.: Modeling evolution of the San Andreas Fault system in northern and central California, Geochemistry, Geophysics, Geosystems, 13, n/a–n/a, https://doi.org/10.1029/2012GC004086, http://dx.doi.org/10.1029/2012GC004086, q08016, 2012.

Quinteros, J. and Sobolev, S. V.: Why has the Nazca plate slowed since the Neogene?, Geology, 41, 32–34, 2013.

Reigber, C., Schmidt, R., Flechtner, F., König, R., Meyer, U., Neumayer, K., Schwintzer, P., and Zhu, S. Y.: An Earth gravity field model complete to degree and order 150 from GRACE: EIGEN-GRACE02S, Journal of Geodynamics, 39, 1–10, https://doi.org/10.1016/j.jog.2004.07.001, 2004.

Reynolds, S. D., Coblentz, D. D., and Hillis, R. R.: Tectonic forces controlling the regional intraplate stress field in continental Australia: Results from new finite element modeling, Journal of Geophysical Research: Solid Earth, 107, 2156–2202, https://doi.org/10.1029/2001JB000408, 2002.

Richards, M. A. and Hager, B. H.: Geoid anomalies in a dynamic Earth, J. Geophys. Res., 89, 5987–6002, 1984.

Richardson, R. M.: Ridge forces, absolute plate motions, and the intraplate stress field, J. Geophys. Res., 97, 11 739–11 748, 1992.

Ritsema, J., Deuss, A., van Heijst, H. J., and Woodhouse, J. H.: S40RTS: a degree-40 shear velocity model for the mantle from new Rayleigh wave dispersion, teleseismic traveltimes, and normal-mode splitting function measurements, Geophys. J. Int., 184, 1223–1236, 2011.

Rogozhina, I., Petrunin, A., Vaughan, A. P. M., Steinberger, B., Johnson, J. V., Kaban, M., Calov, R., Rickers, F., Thomas, M., and Koulakov, I.: Melting at the base of the Greenland Ice Sheet explained by Iceland hotspot history, Nature Geoscience, 9, 366–369, https://doi.org/10.1038/ngeo2689, 2016.

Rychert, K. A., Fischer, K. M., and Rondenay, S.: A sharp lithosphere-asthenosphere boundary imaged beneath eastern North America, Nature, 436, 542–545, 2005.

Schaeffer, A. and Lebedev, S.: Global shear speed structure of the upper mantle and transition zone, Geophys. J. Int., 194, 417–449, 2013.

Schiffer, C. and Nielsen, S.: Implications for anomalous mantle pressure and dynamic topography from lithospheric stress patterns in the North Atlantic Realm, Journal of Geodynamics, 98, 53–69, https://doi.org/10.1016/j.jog.2016.03.014, 2016.

Sobolev, S. V. Popov, A. S. B.: Constraining rheology and water content in the upper mantle by modeling plate tectonics, Geochimica et Cosmochimica Acta, 2009.

Solomon, S. C., Richardson, R. M., and Bergman, E. A.: Tectonic stress: Models and magnitudes, Journal of Geophysical Research: Solid Earth, 85, 6086–6092, https://doi.org/10.1029/JB085iB11p06086, 1980.

Steinberger, B.: Slabs in the lower mantle – results of dynamic modelling compared with tomographic images and the geoid, Phys. Earth Planet. Inter., 118, 241–257, 2000.

Steinberger, B.: Effects of latent heat release at phase boundaries on flow in the Earth's mantle, phase boundary topography and dynamic topography at the Earth's surface, Physics of the Earth and Planetary Interiors, 164, 2 – 20, https://doi.org/10.1016/j.pepi.2007.04.021, 2007.

Steinberger, B.: Topography caused by mantle density variations: observation-based estimates and models derived from tomography and lithosphere thickness, Geophys. J. Int., 205, 604–621, 2016.

Steinberger, B. and Calderwood, A.: Models of large-scale viscous flow in the Earth's mantle with constraints from mineral physics and surface observations, Geophys. J. Int., 167, 1461–1481, 2006.

Steinberger, B., Schmeling, H., and Marquart, G.: Large-scale lithospheric stress field and topography induced by global mantle circulation, Earth Planet. Sci. Lett., 186, 75–91, 2001.

Steinberger, B., Conrad, P. C. Osei Tutu, A., and Hoggard, M. J.: Are superplumes a myth?, TECTON, (in review, TECTON), 2017.

Tesauro, M., Kaban, M. K., and Cloetingh, S. A. P. L.: Global strength and elastic thickness of the lithosphere, Global and Planetary Change, 91, 51–57, 2012.

Thoraval, C. and Richards, M. A.: The geoid constraint in global geodynamics: viscosity structure, mantle heterogeneity models and boundary conditions, Geophys. J. Int., 131, 1–8, https://doi.org/10.1111/j.1365-246X.1997.tb00591.x, 1997.

Thoraval, C., Tommasi, A., and Doin, M.: Plume-lithosphere interaction beneath a fast moving plate, Geophysical Research Letters, 33, L01301, https://doi.org/10.1029/2005GL024047, 2006.

van Hinsbergen, D. J. J., Kapp, P., Dupont-Nivet, G., Lippert, P., DeCelles, P., and Torsvik, T.: Restoration of Cenozoic deformation in Asia, and the size of Greater India, Tectonics, 30, TC5003, https://doi.org/10.1029/2011TC002908, 2011.

Wang, X., Holt, W. E., and Ghosh, A.: Joint modeling of lithosphere and mantle dynamics: Evaluation of constraints from global tomography models, Journal of Geophysical Research: Solid Earth, 120, 8633–8655, https://doi.org/10.1002/2015JB012188, 2015.

Wheeler, P. and White, N.: Quest for dynamic topography: Observations from Southeast Asia, 28, 963–966, https://doi.org/10.1130/0091-7613-2000, 2000.

Wilks, K. R. Carter, N. L.: Rheology of some continental lower crustal rocks, Tectonophysics, 182, 57–77, 1990.

Zhong, S. and Davies, G. F.: Effects of plate and slab viscosities on geoid, Earth Planet. Sci. Lett., 170, 487–496, 1999.

Zoback, M. and Mooney, W.: Lithospheric Buoyancy and Continental Intraplate Stresses, International Geology Review, 45, 95–118, https://doi.org/10.2747/0020-6814.45.2.95, 2003.

Zoback, M. L.: First- and second-order patterns of stress in the lithosphere: The World Stress Map project, J. Geophys. Res., 97, 11 703–11 728, 1992.